Development of Multi-Concentration Ag:Cu Bimetallic Nanoparticles as a Promising Bactericidal for Antibiotic-Resistant Bacteria as Per Molecular Docking Exploration

S. Mureed
Government College University Lahore
S. Naz
Tianjin Institute of Industrial Biotechnology Chinese Academy of Sciences
A. Haider
University of Veterinary and Animal Sciences
A. Raza
Riphah International University - Lahore Campus
A. Ul-Hamid
King Fahd University of Petroleum & Minerals
J. Haider
Tianjin Neurological Institute
muhammad ikram (dr.muhammadikram@gcu.edu.pk)
Government College University Lahore https://orcid.org/0000-0001-7741-789X
R. Ghaffar
University of Education Lahore
M. Irshad
University of Engineering and Technology
A. Ghaffar
Government College University Lahore
A. Saeed
Quaid-i-Azam University

Nano Express

Keywords: Bimetallic, antimicrobial, docking, HR-TEM, Cu:Ag

Posted Date: December 2nd, 2020

DOI: https://doi.org/10.21203/rs.3.rs-115751/v1

Abstract

The present study is concerned with the influence of various concentrations of Ag within Cu:Ag bimetallic nanoparticles developed for use as a promising anti-bacterial agent against antibiotic-resistant bacteria. Here, Cu:Ag bimetallic nanoparticles (NPs) with various concentration ratios (2.5, 5.0, 7.5, and 10 wt.%) of Ag in fixed amount of Cu labeled as 1:0.025, 1:0.050, 1:0.075, and 1:0.1 were synthesized using co-precipitation method with ammonium hydroxide and deionized water as solvent, polyvinyl pyrrolidone as a capping agent, and sodium borohydride and ascorbic acid as reducing agents. These formulated products were characterized through a variety of techniques. XRD confirmed phase purity and detected the presence of distinct fcc structures belonging to Cu and Ag phases. FTIR spectroscopy confirmed the presence of vibrational modes corresponding to various functional groups and recorded characteristic peak emanating from the bimetallic. UV-visible spectroscopy revealed reduction in band gap with increasing Ag content. SEM and HR-TEM micrographs demonstrated spherical morphology of Ag-doped Cu bimetallic with small and large scale agglomerations. The samples exhibited varying dimensions and interlayer spacings. Bactericidal action of synthesized Cu:Ag bimetallic NPs depicted statistically significant ($P < 0.05$) inhibition zones recorded for various concentrations of Ag dopant against *Staphylococcus aureus (S. aureus), Escherichia coli (E. coli),* and *Acinetobacter baumannii (A. baumannii)* ranging from (0.85 – 2.8 mm), (0.55 – 1.95 mm) and (0.65 – 1.85 mm), respectively. Broadly, Cu:Ag bimetallic NPs were found to be more potent against gram-positive compared with gram-negative. Molecular docking study of Ag-Cu bimetallic NPs was performed against β-lactamase which is a key enzyme of cell wall biosynthetic pathway from both *S. aureus* (Binding score: -4.981 kcal/mol) and *A. bauminnii* (Binding score: -4.013 kcal/mol). Similarly, binding interaction analysis against FabI belonging to fatty acid biosynthetic pathway from *A. bauminnii* (Binding score: -3.385 kcal/mol) and *S. aureus* (Binding score: -3.012 kcal/mol) along with FabH from *E. coli* (Binding score: -4.372 kcal/mol) was undertaken. These theoretical computations indicate Cu-Ag bimetallic NPs as possible inhibitor of selected enzymes. It is suggested that exploring in vitro inhibition potential of these materials may open new avenues for antibiotic discovery.

1. Introduction

Casualties resulting from infections caused by antibiotic-resistant bacteria have become a major contributor to human sufferings in the world today. A variety of micro-organisms composed of bacteria, fungi, viruses, and parasites are present within the earth and its environment. These species cause serious complications in the development and use of medical equipment, healthcare goods, food processing, water purification systems, and domestic sanitation [1, 2]. Antibiotics are routinely employed by physicians to kill bacteria that cause illness in humans and animals. The disadvantage of frequent use of antibiotics is that it renders bacteria drug-resistant with time. Antibiotics also serve to reduce the number of ‘good’ bacteria present in the body, which fight against infections. In addition, a few germs are known to be drug-resistant [3-7]. Novel efforts are being made to address the issue of drug-resistant bacteria and substitute current antimicrobial agents with more efficient and complementary therapies. In

this sense, nanotechnology has rendered an enormous contribution to the production of nanomaterials such as metallic and metal oxide NPs (i.e., Ag, Cu, CuO, TiO_2, SiO_2, MgO, and ZnO) to fight an ever-increasing number of antimicrobial-resistant microorganisms. Among these, Cu and Ag NPs have shown encouraging antimicrobial properties [8-12].

In recent years, bimetallic NPs have been developed and used for various applications in the fields of chemistry, material science, biotechnology, and environmental protection. Bimetallic NPs containing copper (Cu) and silver (Ag) with a high fraction of surface atoms and high specific surface area have been widely studied [13]. These bimetallic NPs are of great interest due to their enhanced chemical, optical, catalytic, biological, plasmonic, and especially antimicrobial properties [14-20]. Ag ions can be reduced by ethanol under atmospheric conditions at 800 to 1000 ^{o}C to obtain silver NPs [21, 22]. Silver NPs have good antimicrobial efficacy, therefore, it is used in sunscreen creams and water treatment [23]. Cu NPs are fabricated by the reduction of copper sulfate with hydrazine in ethylene glycol under microwave irradiation, and can also be used as antibacterial agent [24-26].

Metals Cu and Ag individually do not have promising optical, catalytic, and structural properties and cannot be converted into bimetallics. On the other hand, combining both metals (Cu:Ag) offers new opportunities to tune the structure and morphology of this material for desired applications. Based upon its structure such as core-shell, dumb-bell structure, two interface structure, randomly mixed structure, and flower shape structure, various types of bimetallic NPs exhibit antimicrobial activity [27-31]. There are various methods for synthesis of bimetallic NPs including co-precipitation method, sol-gel method, hydrothermal method, reduction method, microemulsion method, and polyol method [32-37].

In this study, Cu:Ag bimetallic NPs were synthesized through co-precipitation method using ammonium hydroxide and deionized water as solvent, polyvinyl pyrrolidone as a capping agent, and sodium borohydride and ascorbic acid as reducing agents. Four samples with various concentrations were prepared. With increasing concentrations of Ag in prepared bimetallic NPs, samples showed better activity against bacteria acinetobacter baumannii that causes fever & nausea. The synthesized material adopted red appearance during rapid growth suggesting that antimicrobial activity was enhanced by increasing concentrations of Ag in bimetallic NPs. Furthermore, *In silico* predictions using molecular docking study were performed to identify the interaction pattern of Cu:Ag bimetallic NPs against *β*-lactamase enzyme of cell wall biosynthetic pathway alongside FabI and FabH enzymes of fatty acid biosynthetic pathway.

2. Experimental Section

2.1 Materials

Copper (II) chloride ($CuCl_2 .2H_2O$, 98.9 %), and silver nitrate ($AgNO_3$) as precursors, polyvinyl pyrrolidone (PVP, an average molecular weight of 40000) as capping agent, sodium borohydride ($NaBH_4$, 99.9%) and

L- Ascorbic acid ($C_6H_8O_6$, 99.0%) as reducing agents and ammonium hydroxide (NH_4OH) were used in the present study upon purchasing from Sigma Aldrich USA.

2.2 Synthesis of Bimetallic Cu:Ag NPs

Bimetallic Cu:Ag NPs were prepared using co-precipitation method as portrayed in Fig. 1. In deionized water, 1.25 g of PVP and 0.5 g of ascorbic acid were added and stirred vigorously at 100 ^oC. Two solutions of 40 mL of ammonium hydroxide were prepared individually; in one solution, 1.7 g copper chloride and in the other solution 1.7 g silver nitrate were added. These two solutions are then added one after the other to the initially prepared solution with the addition of 0.5 g of $NaBH_4$. Afterwards, the final solution was stirred at 100 ^oC for 4 hours to make it homogeneous and centrifuged at 6000 rpm for complete extraction of NPs. The obtained bimetallic NPs were dried at 100 ^oC for complete elimination of moisture and impurities, to make sure that the prepared bimetallic products were in pure form [12]. Similarly, four samples with various Ag concentrations (mol 2.5%, 5%, 7.5%, and 10%) were prepared with fixed Cu ratios.

2.4 Antimicrobial Activity

In vitro bactericidal potential of Cu:Ag bimetallic NPs was evaluated against pathogenic bacteria *S. aureus, E. coli* and *A. baumannii* isolates obtained from bovine mastitic milk using well diffusion method. Mannitol salt agar, MacConkey agar and Lauria Bertani agar were swabbed with isolated bacteria activated growth 1.5×10^8 CFU/ml. After media solidification, five wells were prepared using yellow pipette containing 15 mm diameter and ten microliter (5 µg/mL). Freshly prepared Cu:Ag bimetallic NPs were loaded into wells with different ratios in comparison with ten microliters of amoxicillin (5 µg/mL) as positive control and 50 µl of DIW as negative control. The bactericidal activity of synthesized Cu:Ag bimetallic NPs was determined by measuring inhibition zones (mm) formed after incubation of 15 hours at 37 °C. The bactericidal activity of synthesized NPs was considered statistically significant using SPSS 20.0,one-way analysis of variance (ANOVA) [57].

2.5 Molecular Docking Study

Antibiotics decrease bacterial growth and cause death of bacteria through cell wall damage, disrupting biochemical processes, cell membrane damage, and penetration through biofilm [38]. In recent decades, plenty of nanoparticles with potential bactericidal activity have been reported, which kill bacteria either through cell wall disruption or due to non-availability of the food source following mechanism similar to known antibiotics [39-41]. Hence, enzymes belonging to these biochemical pathways are thought to be an important and attractive target for antibiotic discovery [12]. Here, key enzymes from cell wall biosynthetic pathway were selected (i.e. β-lactamase) and fatty acid biosynthetic pathway (i.e. FabH and FabI) as possible targets to evaluate the mechanism of interaction of Cu:Ag bimetallic NPs with their active pocket as inhibitors (see Fig. 2).

3D structural parameters of selected enzymes were fetched from protein data bank having PDB code: 4U0X (2.03 Å Resolution) for *β*-lactamase [42] and 6AH9; Resolution 1.74 Å [43] for Enoyl-[acyl-carrier-protein] reductase (FabI) from *A. bauminnii*. The *β*-lactamase (3D structure) with PDB ID: 1MWU; Resolution 2.6 Å [44] and FabI with PDB code: 4CV1; Resolution 1.95 [45] from *S. aureus* while for FabH from *E. coli* has PDB code: 4Z8D; Resolution 2.0 Å [46].

Molecular docking study of Cu:Ag bimetallic NPs was performed using ICM Molsoft v3.8–4a or above (Molsoft L.L.C., La Jolla, CA) software to identify binding interactions with key residues of active site [47]. The protein/receptor preparation tool of ICM was used for optimization and structure preparation of selected enzyme targets. Steps involved were addition of polar H-atoms, deletion of water molecules, and energy minimization using default parameters. The co-crystallized ligand molecule was removed to provide room for docking of NPs. The binding pocket was defined using grid box specifying position of crystallized ligand. The conformation with lowest binding energy out of top 10 docked conformations was selected in each case to analyze interaction pattern and binding tendency of Ag-Cu bimetallic NPs inside active pocket. Pymol and discovery studio visualizer software were employed for analysis and 3D-view depiction of binding interactions [48]. The structure of Cu:Ag bimetallic NPs was retrieved from PubChem in .sdf format.

2.6 Characterization

Structural analysis and phase purity were observed by engaging XRD (PAN analytical X'pert pro XRD) with Cu-Kα radiation (λ=0.154 nm, 20˚ to 80˚). The presence of vibrational modes corresponding to various functional groups was evaluated using Fourier transform infrared spectroscopy-FTIR with Perkin Elmer spectrometer. Absorption spectra were acquired using a UV-visible-Genesys 10S spectrophotometer. FESEM coupled with EDS spectrometer (JSM-6610LV) and HR-TEM (JEOL JEM 2100F) was employed to visualize surface morphologies. The ICM v3.8-4a or above (Molsoft L.L.C., La Jolla, CA) software was used for molecular docking analysis.

3. Results And Discussion

XRD analysis was undertaken to assess the composition of phases and crystal structure of formulated products. Fig. 3a reveals the XRD pattern plotted between 20-80˚. In bimetallic Cu:Ag, observed reflections around ~38.2˚, 46˚, 64.4˚, and 77.1˚ are attributed to (111), (200), (220), and (311) facets with fcc phase of Ag according to JCPDS No. 04-0783 [32, 49-52]. Whereas, in case of Cu, diffractions appeared around 32.6˚, 44.2˚, and 51˚ denoted (110), (111), and (200) lattice planes that confirmed the presence of fcc structured CuO and metallic Cu respectively, and well-matched with JCPDS No. 04-0836 [32, 53-56]. In extracted pattern, both Ag and Cu peaks were observed which signifies NPs constituting both Ag and Cu phases. Moreover, the existence of CuO in samples with lower Ag content (e.g., 1:0.025, 1:0.050, and 1:0.075) reveals that Cu NPs have been oxidized and exhibit resistance-less behavior at high-temperature degradation at lower Ag concentrations [52]. Conversely, in the sample with maximum Ag content (1:0.1), CuO peak appears low which indicates the formation of partially oxide-free product [57]. This suggests

that improved oxidation resistance of bimetallic NPs will occur due to the addition of Ag [52]. No additional peak of impurity was detected within the instrument limits while each crystallographic plane comprises energetically distinct sites based on atom density. Both Cu and Ag NPs have high atom density facets at (111) that serve to expose the maximum orientation of planes [51, 58]. Using Bragg's law, d-spacing of Ag and Cu were found to be 0.24 and 0.21 nm respectively, which corresponds to distinct plane (111) of both elements and was in line with HR-TEM findings (Fig. 6) [51, 59-62]. Corresponding SAED rings (Fig. 3b-d) obtained from prepared bimetallic products display distinct ring patterns that demonstrate well-crystallized products and accord well XRD patterns.

FTIR spectra were recorded between 500-4000 cm^{-1} as presented in Fig. 3e; the transmitted band positioned between 600-900 cm^{-1} is caused by the formation of Cu:Ag bonding [63]. The observed band around ~1200 and 1400 cm^{-1} is attributed to C-O and C-H, respectively; peaks appeared around ~1800 and 2100 cm^{-1} corresponds to C=O and N-H bonding due to PVP and NH_4OH [64]. Transmittances observed around ~2800cm^{-1} and 3400cm^{-1} are ascribed to C≡N and presence of hydroxyl group (O-H) [64].

Fig. 4a shows the absorption spectra of Ag-Cu bimetallic NPs with clear absorption bands sited at 340, 410, and 500 nm, which are ascribed to surface plasmonic resonance absorption of metallic Ag and Cu [52]. The band appearing at 410 nm typically arises due to the presence of Ag NPs, and latter peak positioned at 510 nm is attributed to the existence of Cu NPs [52, 57-59, 65-67]. It may be suggested that bimetallic NPs are developed with distinct Ag and Cu phases, instead of bimetallic development that was also affirmed by XRD results as discussed earlier [52]. Slight redshift in absorption band at 410 nm and an increase in maximum absorption with increasing Ag content was observed [58]. Using the Tauc equation,

$$[\alpha hv = K(hv - Eg)^n] \ldots\ldots\ldots (1)$$

where α is considered as coefficient of absorption [2.303 log(T/d), T is transmitted light and d shows thickness of sample cell], h symbolizes Planck's constant ($6.62607015 \times 10^{-34}$ Js), is frequency of light, K shows absorption index, and E_g is equal to band gap energy in eV. The value of "n" is related to electronic transition type of band gap [13, 26, 68, 69]. The band gap of prepared bimetallic products was calculated and found to be 3.2, 2.9, 2.7, and 2.6 eV, as demonstrated in Fig. 4b-e.

From SEM images (Fig. 5a-d) of as-synthesized Cu:Ag bimetallic nanocomposites, it was observed that small-sized particles were deposited on the surface of large particles. As the Ag content was increased from 2.5% to 7.5%, it led to the formation of various particles with different morphology which finally culminated into chunky Cu:Ag NPs. Further, accumulations of uneven and tiny Ag particles are augmented with increasing dopant concentration, which led to more scattered blocks appearing on its surface. This illustrates the major influence of Ag insertion into Cu. The morphology of prepared samples was further confirmed by HR-TEM micrographs (see Fig. 5e-h).

To further elaborate on the morphology and d-spacing of prepared bimetallic, HR-TEM with 10 nm resolution was engaged. In Fig. 6a, d-spacing (0.21 nm) of Cu NPs corresponds to (111) facet of Cu, as also evident in XRD results (Fig. 3a). Fig. 6b portrays a slight increase in layer spacing (0.21 to 0.22 nm) and also shows the Ag NPs with 0.24 nm layer distance matched with (111) plane. Similarly, Fig. 6c-d show calculated layer spacings and separate phases of bimetallic while Fig. 6e demonstrates particle shape of Ag and Cu NPs. The particles in HR-TEM images are seen to possess a core-shell structure [70]. For example in Fig. 6d within a single particle, lattice fringes emanating from Cu and Ag were recorded. This strongly suggests the formation of core-shell bimetallic NPs with different Cu:Ag ratios yielding irregular quasi-spherical NPs. Furthermore, some parts in the TEM image within a particle are dark while some bright. This variation in contrast within a single particle may indicate the presence of two distinct constituent elements suggesting the creation of bimetallic Cu:Ag particles [71, 72].

In vitro bactericidal efficacy of Cu:Ag bimetallic NPs using agar well diffusion assay is presented in Fig. 7a, b, and table 1. The results demonstrate direct proportional relationship between synthesized NPs concentration and inhibition zones (mm). Statistically significant ($P < 0.05$) inhibition zones recorded for (2.5, 5, 7.5 and 10 wt%) Ag dopant against *S. aureus, E. coli* and *A. baumannii* ranged from 0.85 – 2.8 mm, 0.55 – 1.95 mm and 0.65 – 1.85 mm, respectively, see Fig. 6 (a) and table 1. All results compared with DIW (0 mm) and amoxicillin (4 mm) as negative and positive control, respectively. Similarly, %age efficacy of doped NPs increased (21.2 – 70 %), (13.7 – 48.7 %) and (16.2 – 46.2 %) against *S. aureus, E. coli* and *A. baumannii*, respectively Fig. 7a. Overall Cu:Ag bimetallic NPs were found to be more potent against *S. aureus* (i.e. gram +ive) compared with *E. coli* and *A. baumannii* (i.e. gram –ive).

Size, concentration, and shape of NPs directly affect oxidative stress produced by nanostructures. Bactericidal efficacy in the form of inhibition zones (mm) improved due to greater wt% doping of Ag-doped Cu bimetallic NPs due to maximum cations (++) availability. Bactericidal action in regard to size and concentration depicts an inverse relationship to size [58,59]. Nano-sized structures produce reactive oxygen species (ROS) efficiently which reside in bacterial cell membranes leading to extrusion of cell organelles and ultimately death of bacteria [60]. Besides ROS production, cationic interaction of Ag^{+} and Cu^{++} with negatively charged parts of bacteria cell membrane results in improved bactericidal efficacy at increasing concentrations through cell lysis and bacteria collapse [58, 61].

Table 1 Bactericidal action of Cu-Ag bimetallic NPs

Sample	[1]Inhibition zone (mm)	[2]Inhibition zone (mm)	[3]Inhibition zone (mm)	Ampicillin	DIW
	0.005 mg/ml	0.005 mg/ml	0.005 mg/ml	0.005 mg/ml	
1:2.5%	0.85	0.55	0.65	4	0
1:5%	1.45	0.95	1.05	4	0
1:7.5%	2.05	1.45	1.5	4	0
1:10%	2.8	1.95	1.85	4	0

[1] Inhibition zone (mm) of Cu:Ag bimetallic NPs for *S. aureus*

[2] Cu:Ag bimetallic NPs inhibition zones measurements for *E. coli*

[3] Bimetallic NPs zones of inhibition (mm) for *A. baumannii*

Biological applications of various classes of nanoparticles have been extensively studied since the last few decades. Owing to unique characteristics of NPs, they have been extensively utilized for their potential as bactericidal agent with the ability to substitute traditional antibiotics. NPs interact with bacterial cells, disrupt cell membrane permeation and destroy key metabolic pathways [73]. The specific mechanism of nanoparticle toxicity towards bacteria need to be explored. It is believed that NPs interact with bacterial cell involving electrostatic forces, van der Waals forces or hydrophobic interactions that ultimately result in death of bacteria. Enzymes have been reported as main virulence factor involved in bacterial infection and targeting them to inhibit their activity aid in tackling the caused infection [74]. Here, molecular docking study of Cu:Ag NPs against enzyme targets of cell wall alongside fatty acid biosynthetic pathway identified binding interaction pattern of these NPs inside active pocket. Keeping in view in vitro antibacterial potential of these NPs against *A. bauminnii*, *S. aureus* and *E. coli*, the enzyme targets were selected from these microorganism to get an insight into possible mechanism behind their bactericidal activity.

Best docked conformation observed in case of Cu:Ag Bimetallic NPs with *β*-lactamase from *A. bauminnii* revealed hydrogen bonding interaction with Glu272 (2.8 Å) and Ser286 (3.2 Å) along with metal contact interaction with Val292 and the docking score was -4.013 kcal/mol (Fig. 8a). Similarly, binding score of Ag-Cu bimetallic NPs observed against *β*-lactamase from *S. aureus* was -4.981 kcal/mol possessing H-bonding interaction with Ser403 (3.2 Å), Tyr519 (3.6 Å), Gln521 (3.0 Å) and Asn464 (3.1 Å) as shown in Fig. 8b.

Second enzyme target selected in the current study FabI belong to fatty acid biosynthetic pathway and molecular docking predictions suggested Cu:Ag bimetallic NPs as potential inhibitor against this target. The Cu:Ag Bimetallic NPs showed good binding score (-3.385 kcal/mol) against FabI from A. bauminnii having H-bonding with Ser201 (2.7 Å), Ala199 (3.5 Å), and Leu198 (3.3 Å) as depicted in Fig. 9a. Similarly,

best docked conformation of Ag-Cu NPs with active site of FabI from S. aureus showed H-bonding with Gly202 (2.5 Å)and Gln155 (2.5 Å) having binding score -3.012 kcal/mol (Fig. 9b).

4. Conclusion

Cu:Ag bimetallic nanoparticles were prepared through co-precipitation method for use in applications to combat bacteria-related ailments. XRD profiles confirmed the presence of fcc structured CuO and metallic Cu and Ag particles. Both Ag and Cu peaks were observed which signifies bimetallic NPs entailing Ag and Cu phases. Planes observed in XRD analysis correspond well to SAED rings. Attached chemical groups with formulated products and characteristic transmittance band between 600-900 cm^{-1} was caused by the formation of Cu:Ag bonding. The plotted spectra of UV-vis showed absorption at 410 nm which typically arises due to the presence of Ag NPs, and latter peak positioned at 510 nm was attributed to the existence of Cu NPs. The particles in HR-TEM images were seen to have a core-shell structure. Cu:Ag NPs clearly showed the formation of bimetallic NPs with different Cu:Ag ratios yielding irregular quasi-spherical NPs. Further, d-spacing of Cu NPs i.e., 0.21 nm corresponds to (111) facet of Cu detected in XRD results. A slight increase in layer spacing (from 0.21 to 0.22 nm) also shows that Ag NPs with 0.24 nm layer distance matched with (111) plane. Molecular docking study showed good agreement with in vitro bactericidal activity. The binding tendency of Cu:Ag bimetallic NPs against β-lactamase enzyme of cell wall biosynthetic pathway alongside FabI and FabH enzymes of fatty acid biosynthetic pathway demonstrated their inhibition potential that need to be explored further through enzyme inhibition studies.

Abbreviations

Energy dispersive x-ray spectroscopy (EDS), Fourier transform infrared spectroscopy (FTIR), gram-positive (G +ve) and gram negative (G –ve), high resolution transmission electron microscopy (HR-TEM). JCPDS: Joint committee on powder diffraction standards, Silver (Ag), ultra-violet visible spectroscopy (UV-Vis), x-ray diffraction (XRD).

Declarations

ACKNOWLEDGMENT

Authors are thankful to 44ORIC/19 GCU Lahore and Higher Education Commission, HEC through start research grant project # 21-1669/SRGP/R&D/HEC/2017 Pakistan for financial support. Support provided by the Research Institute at the King Fahd University of Petroleum & Minerals, Dhahran, Saudi Arabia is greatly appreciated.

AUTHORS' CONTRIBUTIONS

SM and MI performed the whole experiments and AR wrote the manuscript. AG and RG provided the novel idea to carry out the experiment. AH performed antimicrobial and SA and JH participated in molecular docking study. participated in the data analysis of the results and discussion portion. M. Irshad and AS

reviewed the manuscript, corrected the English. AUH carried out the FESEM and HRTEM analysis. All authors read and approved the final manuscript.

Availability of Data and Materials

All data are fully available without restriction.

Conflict of Interest: Authors confirm that this manuscript has no conflict of interest.

References

[1] Z. Ma, D. Kim, A. T. Adesogan, S. Ko, K. Galvao, and K. C. Jeong, "Chitosan Microparticles Exert Broad-Spectrum Antimicrobial Activity against Antibiotic-Resistant Micro-organisms without Increasing Resistance," *ACS Applied Materials & Interfaces,* vol. 8, no. 17, pp. 10700-10709, 2016/05/04 2016.

[2] J. Niu, Y. Sun, F. Wang, C. Zhao, J. Ren, and X. Qu, "Photomodulated Nanozyme Used for a Gram-Selective Antimicrobial," *Chemistry of Materials,* vol. 30, no. 20, pp. 7027-7033, 2018/10/23 2018.

[3] A. Gupta, S. Mumtaz, C.-H. Li, I. Hussain, and V. M. J. C. S. R. Rotello, "Combatting antibiotic-resistant bacteria using nanomaterials," vol. 48, no. 2, pp. 415-427, 2019.

[4] X. Zhao *et al.*, "Smart Ti3C2Tx MXene Fabric with Fast Humidity Response and Joule Heating for Healthcare and Medical Therapy Applications," *ACS Nano,* 2020/07/09 2020.

[5] Z. Gu *et al.*, "Exploring the Nanotoxicology of MoS2: A Study on the Interaction of MoS2 Nanoflakes and K+ Channels," *ACS Nano,* vol. 12, no. 1, pp. 705-717, 2018/01/23 2018.

[6] W. Yin *et al.*, "Functionalized Nano-MoS2 with Peroxidase Catalytic and Near-Infrared Photothermal Activities for Safe and Synergetic Wound Antibacterial Applications," *ACS Nano,* vol. 10, no. 12, pp. 11000-11011, 2016/12/27 2016.

[7] F. Cao *et al.*, "An Efficient and Benign Antimicrobial Depot Based on Silver-Infused MoS2," *ACS Nano,* vol. 11, no. 5, pp. 4651-4659, 2017/05/23 2017.

[8] J. P. Ruparelia, A. K. Chatterjee, S. P. Duttagupta, and S. J. A. b. Mukherji, "Strain specificity in antimicrobial activity of silver and copper nanoparticles," vol. 4, no. 3, pp. 707-716, 2008.

[9] N. M. Zain, A. Stapley, and G. J. C. p. Shama, "Green synthesis of silver and copper nanoparticles using ascorbic acid and chitosan for antimicrobial applications," vol. 112, pp. 195-202, 2014.

[10] M. Valodkar, S. Modi, A. Pal, and S. J. M. R. B. Thakore, "Synthesis and anti-bacterial activity of Cu, Ag and Cu–Ag alloy nanoparticles: a green approach," vol. 46, no. 3, pp. 384-389, 2011.

[11] A. K. Chatterjee, R. Chakraborty, and T. J. N. Basu, "Mechanism of antibacterial activity of copper nanoparticles," vol. 25, no. 13, p. 135101, 2014.

[12] M. Ikram *et al.*, "Bimetallic Ag/Cu incorporated into chemically exfoliated MoS2 nanosheets to enhance its antibacterial potential: in silico molecular docking studies," *Nanotechnology,* vol. 31, no. 27, p. 275704, Apr 17 2020.

[13] M. Ikram, M. I. Khan, A. Raza, M. Imran, A. Ul-Hamid, and S. Ali, "Outstanding performance of silver-decorated MoS2 nanopetals used as nanocatalyst for synthetic dye degradation," *Physica E: Low-dimensional Systems and Nanostructures,* vol. 124, 2020.

[14] N. Toshima and T. J. N. J. o. C. Yonezawa, "Bimetallic nanoparticles—novel materials for chemical and physical applications," vol. 22, no. 11, pp. 1179-1201, 1998.

[15] N. Toshima, "Capped bimetallic and trimetallic nanoparticles for catalysis and information technology," in *Macromolecular symposia*, 2008, vol. 270, no. 1, pp. 27-39: Wiley Online Library.

[16] P. Venkatesan and J. J. L. Santhanalakshmi, "Designed synthesis of Au/Ag/Pd trimetallic nanoparticle-based catalysts for Sonogashira coupling reactions," vol. 26, no. 14, pp. 12225-12229, 2010.

[17] A. Perdikaki *et al.*, "Ag and Cu Monometallic and Ag/Cu Bimetallic Nanoparticle–Graphene Composites with Enhanced Antibacterial Performance," *ACS Applied Materials & Interfaces,* vol. 8, no. 41, pp. 27498-27510, 2016/10/19 2016.

[18] G. Nazeruddin, R. Prasad, Y. Shaikh, and A. J. D. P. L. Shaikh, "Synergetic effect of Ag-Cu bimetallic nanoparticles on antimicrobial activity," vol. 3, pp. 129-36, 2014.

[19] K. J. Rao and S. Paria, "Mixed Phytochemicals Mediated Synthesis of Multifunctional Ag–Au–Pd Nanoparticles for Glucose Oxidation and Antimicrobial Applications," *ACS Applied Materials & Interfaces,* vol. 7, no. 25, pp. 14018-14025, 2015/07/01 2015.

[20] X. Chen *et al.*, "Enhanced Antimicrobial Efficacy of Bimetallic Porous CuO Microspheres Decorated with Ag Nanoparticles," *ACS Applied Materials & Interfaces,* vol. 9, no. 45, pp. 39165-39173, 2017/11/15 2017.

[21] R. Das, S. Nath, D. Chakdar, G. Gope, and R. J. J. o. n. Bhattacharjee, "Preparation of silver nanoparticles and their characterization," vol. 5, pp. 1-6, 2009.

[22] R. Das, S. S. Nath, D. Chakdar, G. Gope, and R. J. J. o. E. N. Bhattacharjee, "Synthesis of silver nanoparticles and their optical properties," vol. 5, no. 4, pp. 357-362, 2010.

[23] E. Sánchez-López *et al.*, "Metal-based nanoparticles as antimicrobial agents: an overview," vol. 10, no. 2, p. 292, 2020.

[24] H. Zhu, C. Zhang, and Y. J. N. Yin, "Novel synthesis of copper nanoparticles: influence of the synthesis conditions on the particle size," vol. 16, no. 12, p. 3079, 2005.

[25] A. Raza *et al.*, "Enhanced industrial dye degradation using Co doped in chemically exfoliated MoS2 nanosheets," *Applied Nanoscience,* vol. 10, no. 5, pp. 1535-1544, 2019.

[26] A. Raza *et al.*, "A comparative study of dirac 2D materials, TMDCs and 2D insulators with regard to their structures and photocatalytic/sonophotocatalytic behavior," *Applied Nanoscience,* 2020.

[27] K. Tahir *et al.*, "Visible light photo catalytic inactivation of bacteria and photo degradation of methylene blue with Ag/TiO2 nanocomposite prepared by a novel method," vol. 162, pp. 189-198, 2016.

[28] S. Salari, S. A. A. Mousavi, S. Hadizadeh, and A. J. M. p. Izadi, "Epidemiology of dermatomycoses in Kerman province, southeast of Iran: a 10-years retrospective study (2004–2014)," vol. 110, pp. 561-567, 2017.

[29] S. Thota, Y. Wang, and J. Zhao, "Colloidal Au–Cu alloy nanoparticles: synthesis, optical properties and applications," *Materials Chemistry Frontiers,* 10.1039/C7QM00538E vol. 2, no. 6, pp. 1074-1089, 2018.

[30] S. Duan and R. Wang, "Bimetallic nanostructures with magnetic and noble metals and their physicochemical applications," *Progress in Natural Science: Materials International,* vol. 23, no. 2, pp. 113-126, 2013/04/01/ 2013.

[31] M. Ikram *et al.*, "2D chemically exfoliated hexagonal boron nitride (hBN) nanosheets doped with Ni: synthesis, properties and catalytic application for the treatment of industrial wastewater," *Applied Nanoscience,* vol. 10, no. 9, pp. 3525-3528, 2020/09/01 2020.

[32] X. Liu, Y. Wu, G. Xie, Z. Wang, Y. Li, and Q. J. I. J. E. S. Li, "New Green Soft Chemistry Route to Ag-Cu Bimetallic Nanomaterials," vol. 12, pp. 3275-3282, 2017.

[33] K. McNamara and S. A. J. P. c. c. p. Tofail, "Nanosystems: the use of nanoalloys, metallic, bimetallic, and magnetic nanoparticles in biomedical applications," vol. 17, no. 42, pp. 27981-27995, 2015.

[34] J. Huang, L. Lin, D. Sun, H. Chen, D. Yang, and Q. Li, "Bio-inspired synthesis of metal nanomaterials and applications," *Chemical Society Reviews,* 10.1039/C5CS00133A vol. 44, no. 17, pp. 6330-6374, 2015.

[35] C. N. R. Rao, H. S. S. Ramakrishna Matte, R. Voggu, and A. Govindaraj, "Recent progress in the synthesis of inorganic nanoparticles," *Dalton Transactions,* 10.1039/C2DT12266A vol. 41, no. 17, pp. 5089-5120, 2012.

[36] M. Ikram *et al.*, "Photocatalytic and bactericidal properties and molecular docking analysis of TiO2 nanoparticles conjugated with Zr for environmental remediation," *RSC Advances,* 10.1039/D0RA05862A vol. 10, no. 50, pp. 30007-30024, 2020.

[37] M. Ikram *et al.*, "Dye degradation performance, bactericidal behavior and molecular docking analysis of Cu-doped TiO2 nanoparticles," *RSC Advances,* vol. 10, no. 41, pp. 24215-24233, 2020.

[38] T. C. Dakal, A. Kumar, R. S. Majumdar, and V. Yadav, "Mechanistic basis of antimicrobial actions of silver nanoparticles," *Frontiers in microbiology,* vol. 7, p. 1831, 2016.

[39] M. Rai, S. Deshmukh, A. Ingle, and A. Gade, "Silver nanoparticles: the powerful nanoweapon against multidrug-resistant bacteria," *Journal of applied microbiology,* vol. 112, no. 5, pp. 841-852, 2012.

[40] R. J. White, K. Cutting, and A. Kingsley, "Topical antimicrobials in the control of wound bioburden," *Ostomy/wound management,* vol. 52, no. 8, pp. 26-58, 2006.

[41] N.-Y. Lee, P.-R. Hsueh, and W.-C. Ko, "Nanoparticles in the treatment of infections caused by multidrug-resistant organisms," *Frontiers in Pharmacology,* vol. 10, p. 1153, 2019.

[42] R. A. Powers *et al.*, "Biochemical and structural analysis of inhibitors targeting the ADC-7 cephalosporinase of Acinetobacter baumannii," *Biochemistry,* vol. 53, no. 48, pp. 7670-7679, 2014.

[43] *Crystal structure of enoyl-ACP reductase from Acinetobacter baumannii in complex with NAD and Triclosan*. http://www.rcsb.org/structure/6AH9.

[44] D. Lim and N. C. Strynadka, "Structural basis for the β lactam resistance of PBP2a from methicillin-resistant Staphylococcus aureus," *Nature structural biology,* vol. 9, no. 11, pp. 870-876, 2002.

[45] J. Schiebel *et al.*, "Rational design of broad spectrum antibacterial activity based on a clinically relevant enoyl-acyl carrier protein (ACP) reductase inhibitor," *Journal of Biological Chemistry,* vol. 289, no. 23, pp. 15987-16005, 2014.

[46] D. C. McKinney *et al.*, "Antibacterial FabH inhibitors with mode of action validated in Haemophilus influenzae by in vitro resistance mutation mapping," *ACS infectious diseases,* vol. 2, no. 7, pp. 456-464, 2016.

[47] R. Abagyan and M. Totrov, "Biased probability Monte Carlo conformational searches and electrostatic calculations for peptides and proteins," *Journal of molecular biology,* vol. 235, no. 3, pp. 983-1002, 1994.

[48] D. Systemes, "BIOVIA, discovery studio modeling environment. Release 4.5," *Dassault Systemes: San Diego, CA,* 2015.

[49] Y. Li, S. Guo, H. Yang, Y. Chao, S. Jiang, and C. J. R. a. Wang, "One-step synthesis of ultra-long silver nanowires of over 100 μm and their application in flexible transparent conductive films," vol. 8, no. 15, pp. 8057-8063, 2018.

[50] A. S. Lanje, S. J. Sharma, and R. B. J. J. C. P. R. Pode, "Synthesis of silver nanoparticles: a safer alternative to conventional antimicrobial and antibacterial agents," vol. 2, no. 3, pp. 478-483, 2010.

[51] Z. Khan and A. Y. J. R. a. Obaid, "Seedless, copper-induced synthesis of stable Ag/Cu bimetallic nanoparticles and their optical properties," vol. 6, no. 35, pp. 29116-29126, 2016.

[52] Z. Chen, D. Mochizuki, M. M. Maitani, and Y. J. N. Wada, "Facile synthesis of bimetallic Cu–Ag nanoparticles under microwave irradiation and their oxidation resistance," vol. 24, no. 26, p. 265602, 2013.

[53] M. Ahamed, H. A. Alhadlaq, M. Khan, P. Karuppiah, and N. A. J. J. o. N. Al-Dhabi, "Synthesis, characterization, and antimicrobial activity of copper oxide nanoparticles," vol. 2014, 2014.

[54] A. K. Sasmal, S. Dutta, and T. J. D. T. Pal, "A ternary Cu 2 O–Cu–CuO nanocomposite: a catalyst with intriguing activity," vol. 45, no. 7, pp. 3139-3150, 2016.

[55] R. Betancourt-Galindo *et al.*, "Synthesis of copper nanoparticles by thermal decomposition and their antimicrobial properties," vol. 2014, 2014.

[56] D. Mardiansyah *et al.*, "Effect of temperature on the oxidation of Cu nanowires and development of an easy to produce, oxidation-resistant transparent conducting electrode using a PEDOT: PSS coating," vol. 8, no. 1, pp. 1-9, 2018.

[57] L. Rout, A. Kumar, R. S. Dhaka, and P. J. R. a. Dash, "Bimetallic Ag–Cu alloy nanoparticles as a highly active catalyst for the enamination of 1, 3-dicarbonyl compounds," vol. 6, no. 55, pp. 49923-49940, 2016.

[58] L.-u. Rahman *et al.*, "Monitoring of 2-butanone using a Ag–Cu bimetallic alloy nanoscale electrochemical sensor," vol. 5, no. 55, pp. 44427-44434, 2015.

[59] M. K. Singh, P. Manda, A. Singh, and R. J. A. A. Mandal, "Localized surface plasmon behavior of Ag-Cu alloy nanoparticles stabilized by rice-starch and gelatin," vol. 5, no. 10, p. 107108, 2015.

[60] A. H. Zewail and J. M. Thomas, *4D electron microscopy: imaging in space and time*. World Scientific, 2010.

[61] T. N. J. I. Edison, E. R. Baral, Y. R. Lee, and S. H. Kim, "Biogenic Synthesis of Silver Nanoparticles Using Cnidium officinale Extract and Their Catalytic Reduction of 4-Nitroaniline," *Journal of Cluster Science,* vol. 27, no. 1, pp. 285-298, 2016/01/01 2016.

[62] T. Theivasanthi and M. J. a. p. a. Alagar, "Electrolytic synthesis and characterizations of silver nanopowder," 2011.

[63] M. Ismail *et al.*, "Green synthesis of antibacterial bimetallic Ag–Cu nanoparticles for catalytic reduction of persistent organic pollutants," vol. 29, no. 24, pp. 20840-20855, 2018.

[64] M. Banik, M. Patra, D. Dutta, R. Mukherjee, and T. J. N. Basu, "A simple robust method of synthesis of copper–silver core–shell nano-particle: evaluation of its structural and chemical properties with anticancer potency," vol. 29, no. 32, p. 325102, 2018.

[65] D. C. Trinh, T. M. D. Dang, K. K. Huynh, E. Fribourg-Blanc, M. C. J. A. i. N. S. N. Dang, and Nanotechnology, "Synthesis of Cu core Ag shell nanoparticles using chemical reduction method," vol. 6, no. 2, p. 025018, 2015.

[66] M. Tsuji, S. Hikino, R. Tanabe, and Y. J. C. l. Sano, "Synthesis of bicompartmental Ag/Cu nanoparticles using a two-step polyol process," vol. 38, no. 8, pp. 860-861, 2009.

[67] M. Paszkiewicz, A. Gołąbiewska, Ł. Rajski, E. Kowal, A. Sajdak, and A. J. J. o. N. Zaleska-Medynska, "Synthesis and characterization of monometallic (Ag, Cu) and bimetallic Ag-Cu particles for antibacterial and antifungal applications," vol. 2016, 2016.

[68] J. Hassan, M. Ikram, A. Ul-Hamid, M. Imran, M. Aqeel, and S. Ali, "Application of Chemically Exfoliated Boron Nitride Nanosheets Doped with Co to Remove Organic Pollutants Rapidly from Textile Water," *Nanoscale Research Letters,* vol. 15, no. 1, 2020.

[69] M. Ikram, A. Raza, M. Imran, A. Ul-Hamid, A. Shahbaz, and S. Ali, "Hydrothermal Synthesis of Silver Decorated Reduced Graphene Oxide (rGO) Nanoflakes with Effective Photocatalytic Activity for Wastewater Treatment," *Nanoscale Res Lett,* vol. 15, no. 1, p. 95, Apr 28 2020.

[70] Xiong, Ziye (2017) *AG-CU BIMETALLIC NANOPARTICLE SYNTHESIS AND PROPERTIES.* Doctoral Dissertation, University of Pittsburgh.

http://d-scholarship.pitt.edu/32044/13/Xiongz2017etd.pdf

[71] J.-P. Lee *et al.*, "Well-organized raspberry-like Ag@ Cu bimetal nanoparticles for highly reliable and reproducible surface-enhanced Raman scattering," vol. 5, no. 23, pp. 11620-11624, 2013.

[72] W. A. El-Yazeed and A. I. J. R. a. Ahmed, "Monometallic and bimetallic Cu–Ag MOF/MCM-41 composites: structural characterization and catalytic activity," vol. 9, no. 33, pp. 18803-18813, 2019.

[73] A. Thill *et al.*, "Cytotoxicity of CeO2 nanoparticles for Escherichia coli. Physico-chemical insight of the cytotoxicity mechanism," *Environmental science & technology,* vol. 40, no. 19, pp. 6151-6156, 2006.

[74] I. Konieczna *et al.*, "Bacterial urease and its role in long-lasting human diseases," *Current Protein and Peptide Science,* vol. 13, no. 8, pp. 789-806, 2012.

Figures

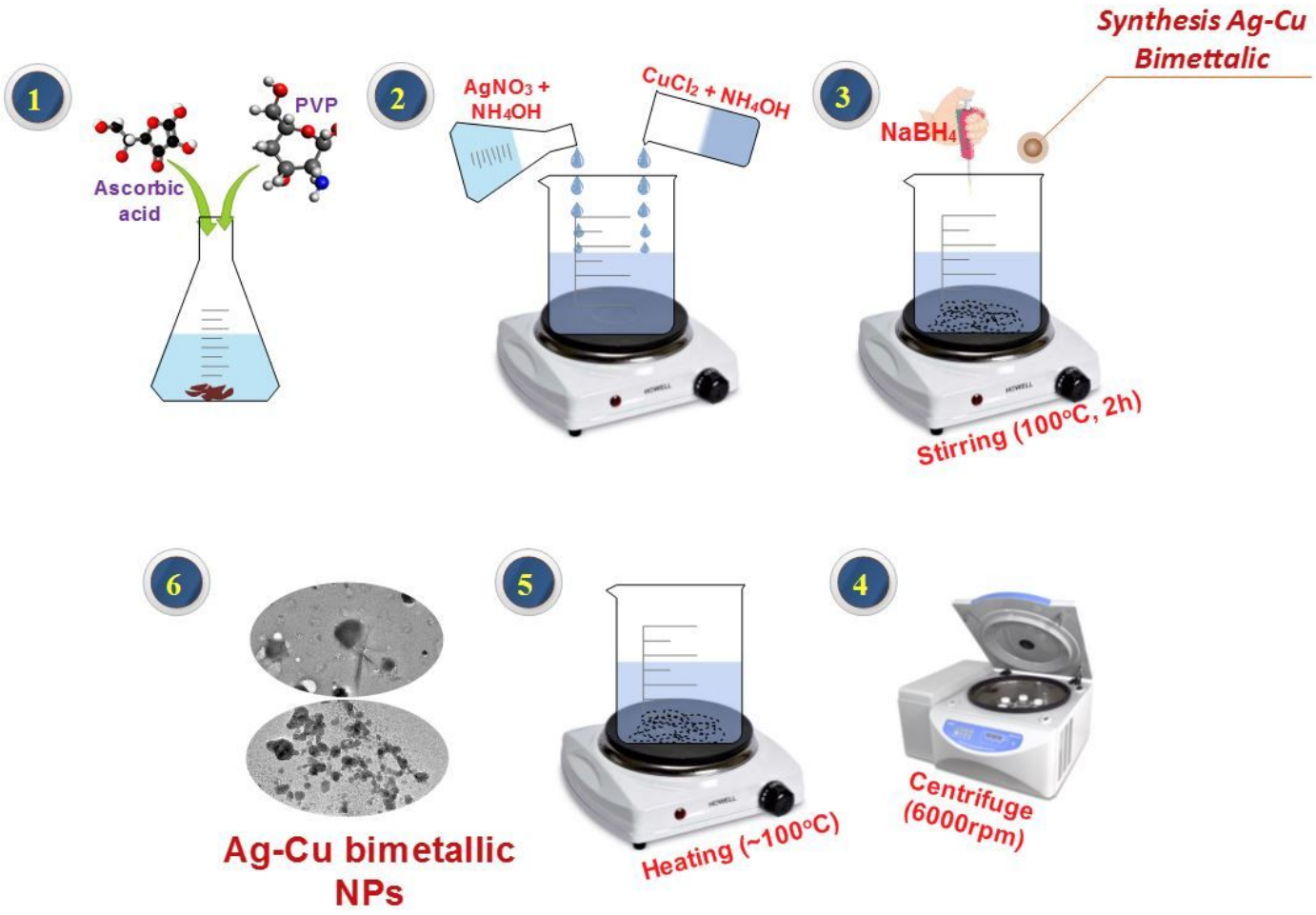

Figure 1

Illustration showing synthesis of Cu:Ag bimetallic NPs

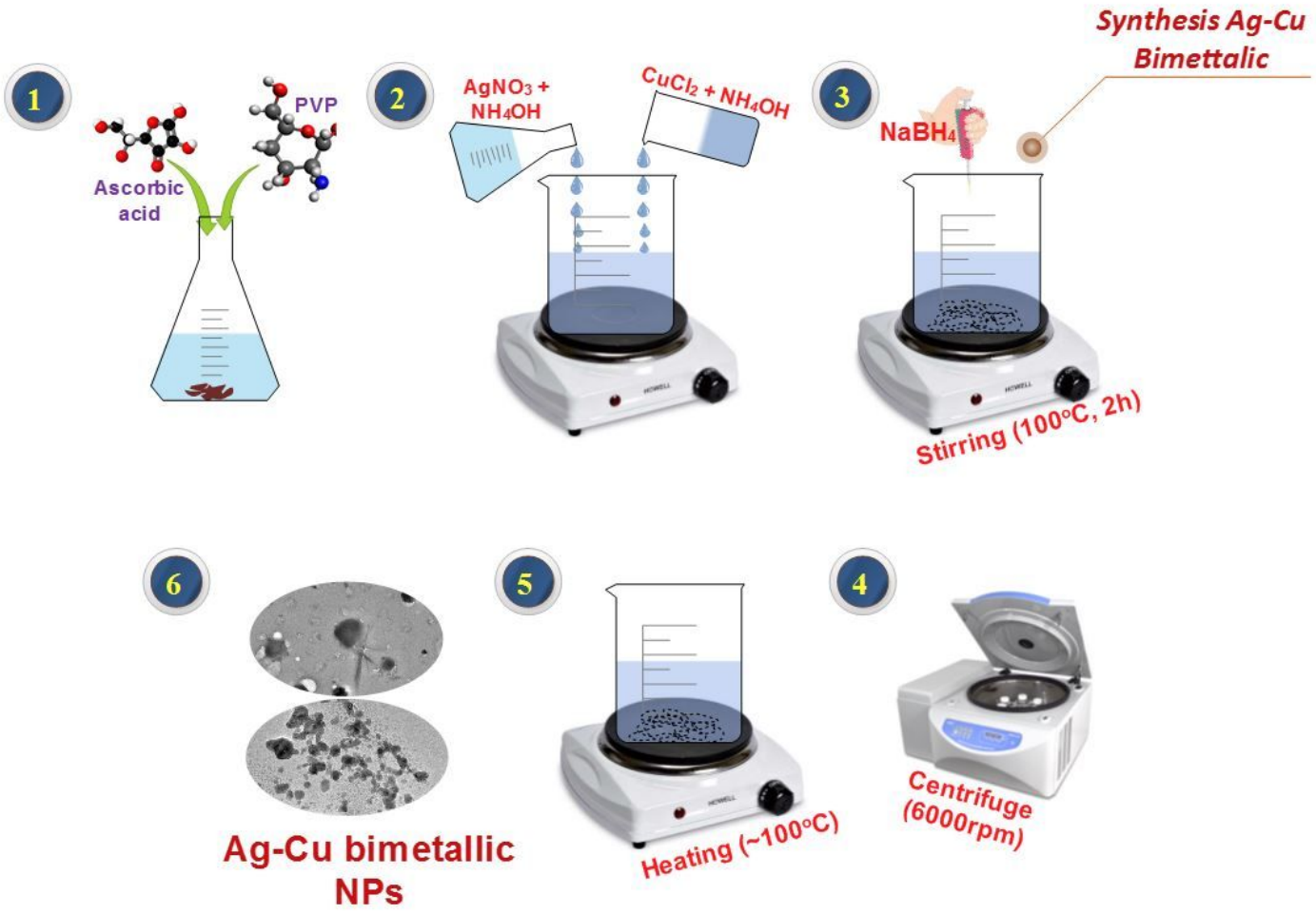

Figure 1

Illustration showing synthesis of Cu:Ag bimetallic NPs

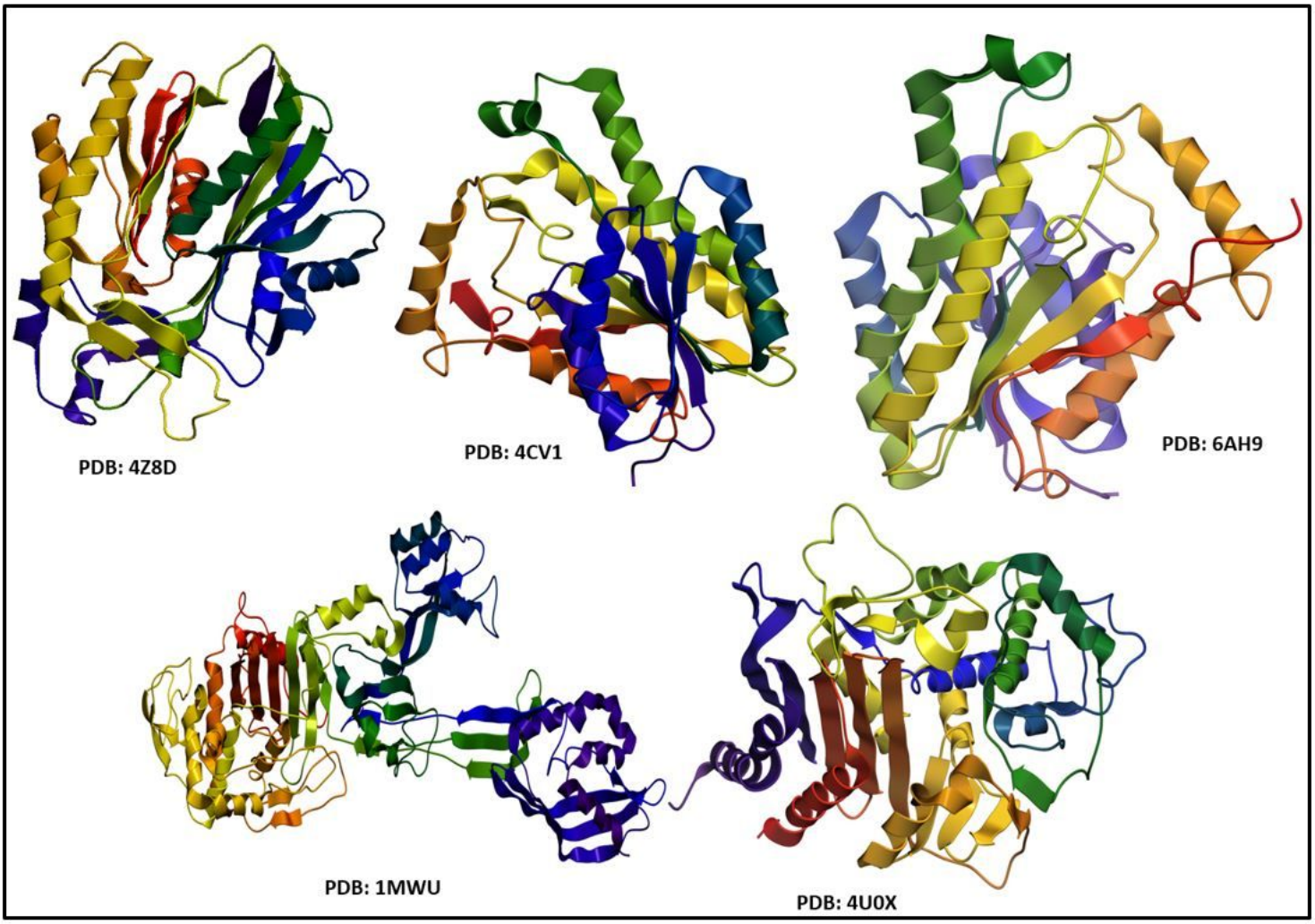

Figure 2

3D-structure of protein targets β-lactamase, FabI (From A. bauminnii & S. aureus) and FabH from E. coli

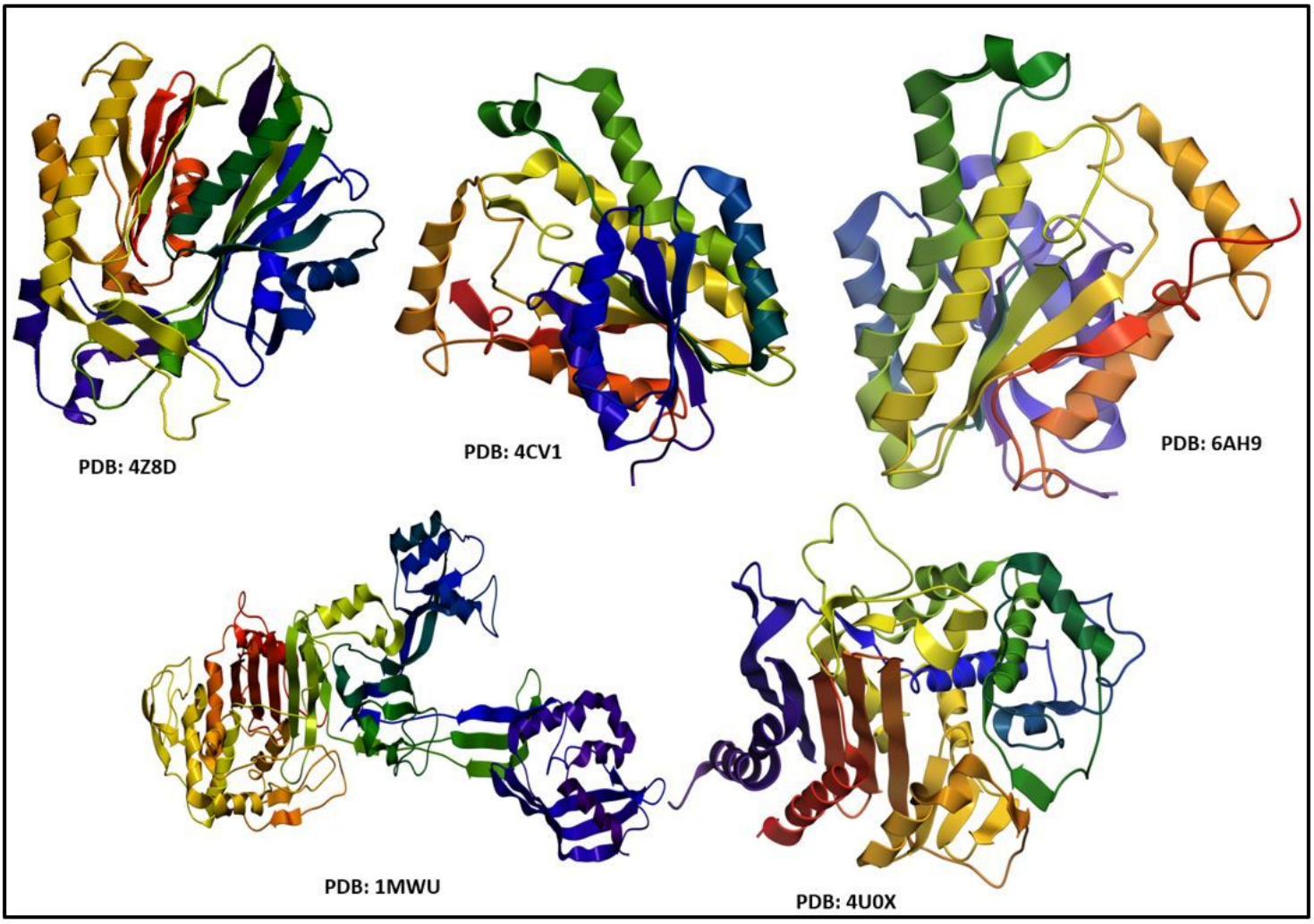

Figure 2

3D-structure of protein targets β-lactamase, FabI (From A. bauminnii & S. aureus) and FabH from E. coli

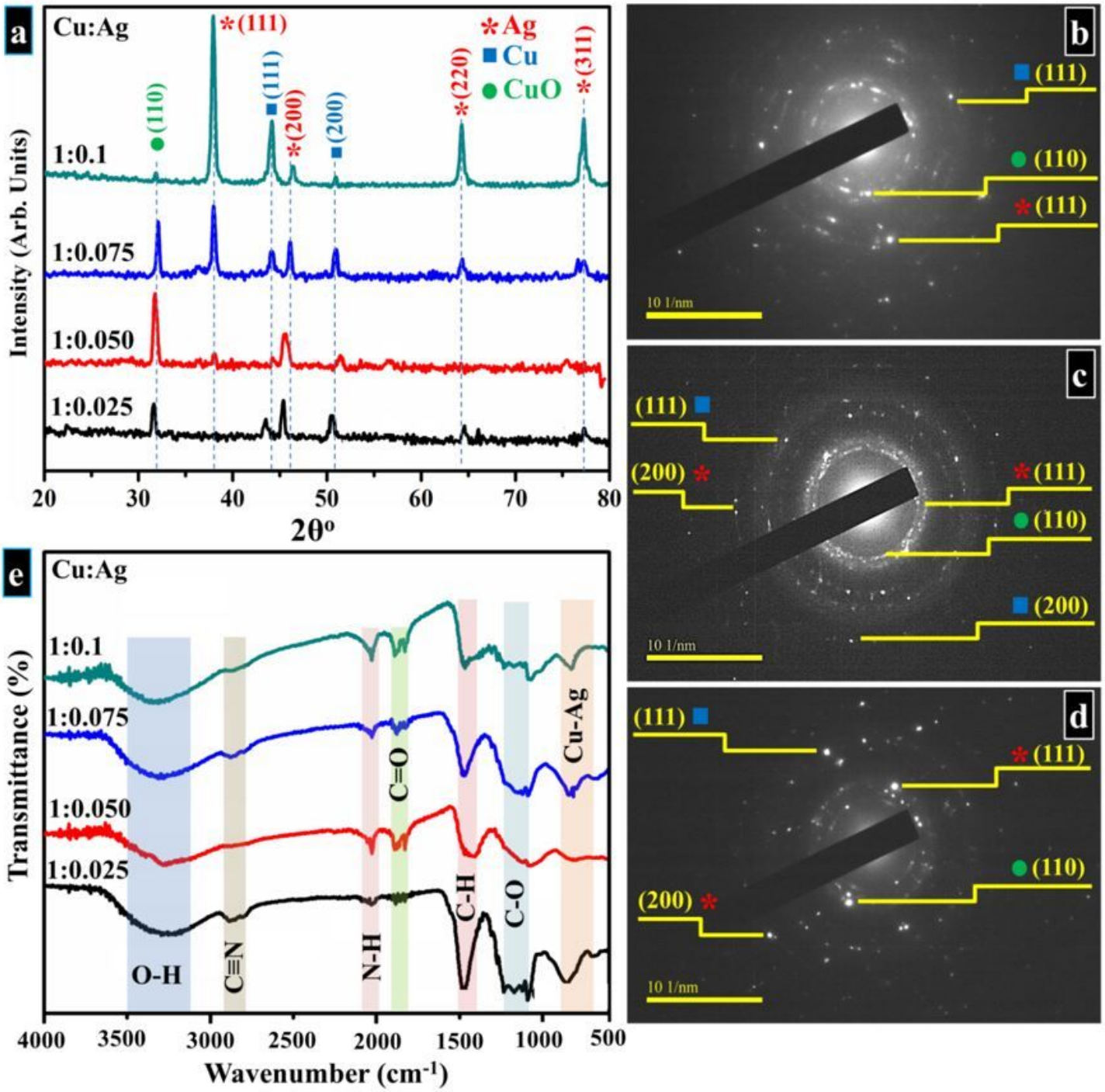

Figure 3

(a) XRD profiles obtained from Cu:Ag bimetallic NPs (b-d) SAED rings obtained using HR-TEM for samples (b) 1:0.025, (c) 1:0.050, and (d) 1:0.10 (e) FTIR spectra of prepared samples.

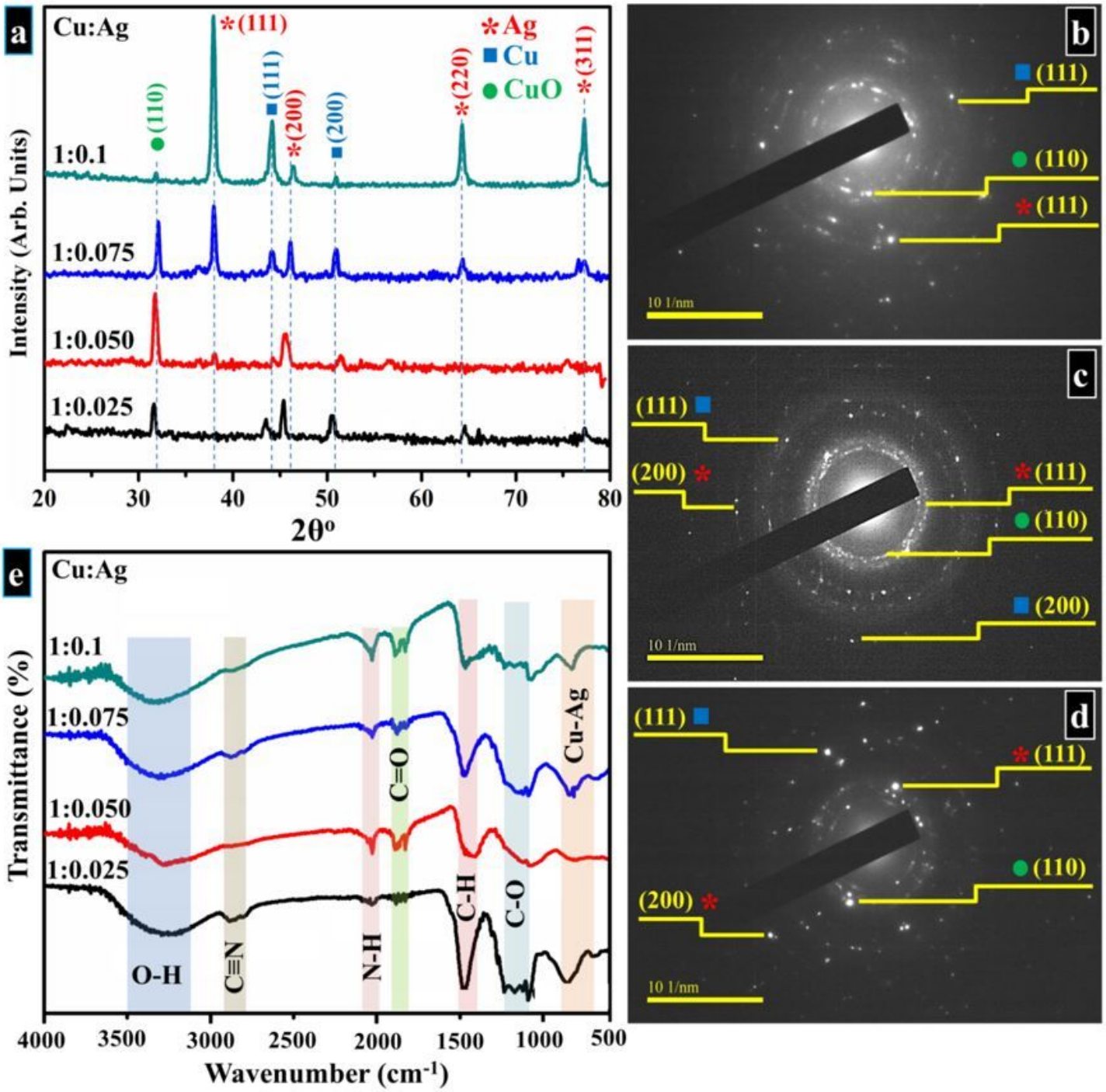

Figure 3

(a) XRD profiles obtained from Cu:Ag bimetallic NPs (b-d) SAED rings obtained using HR-TEM for samples (b) 1:0.025, (c) 1:0.050, and (d) 1:0.10 (e) FTIR spectra of prepared samples.

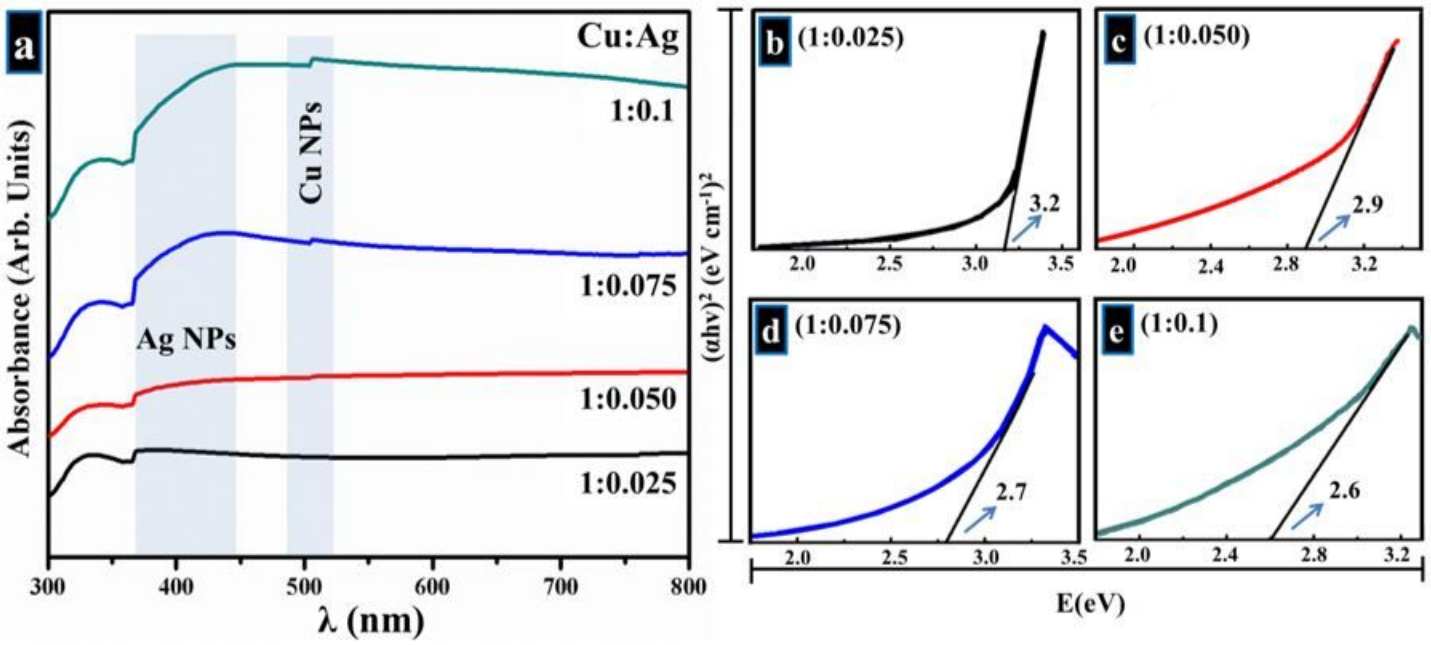

Figure 4

UV-vis spectra obtained from bimetallic (b-e) Tauc plot analysis

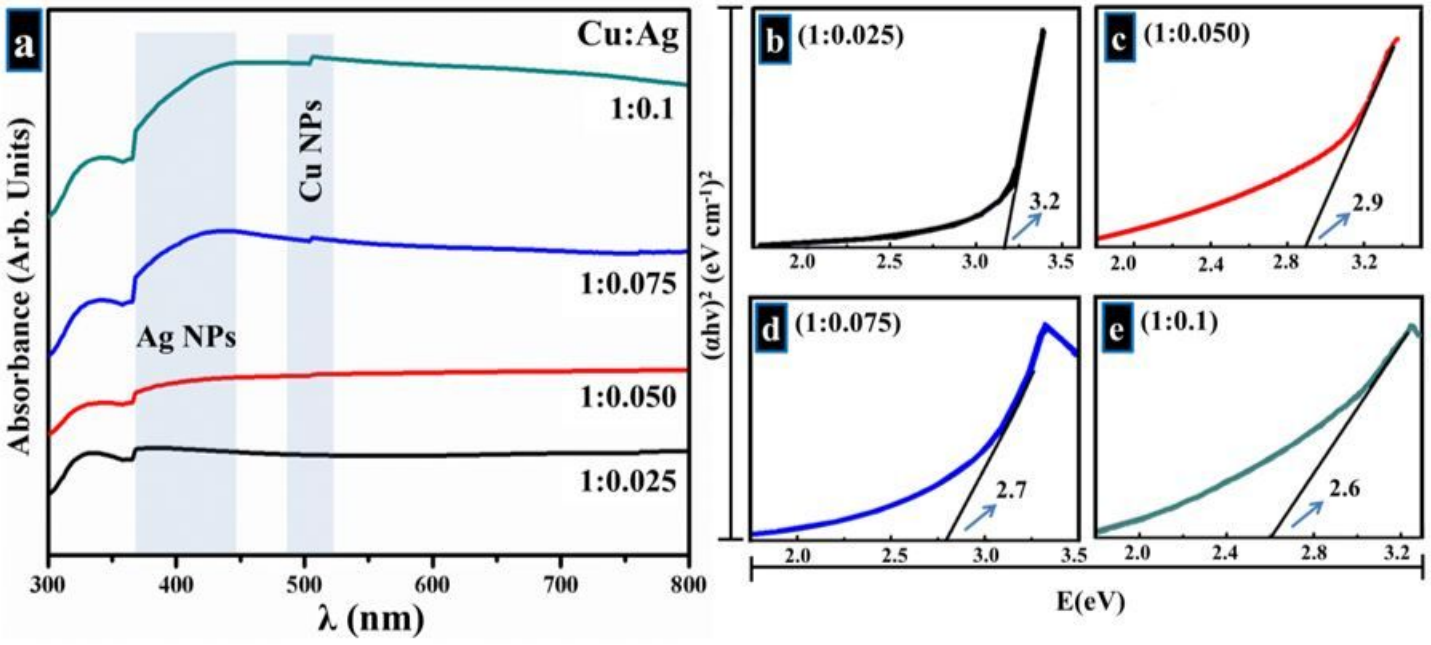

Figure 4

UV-vis spectra obtained from bimetallic (b-e) Tauc plot analysis

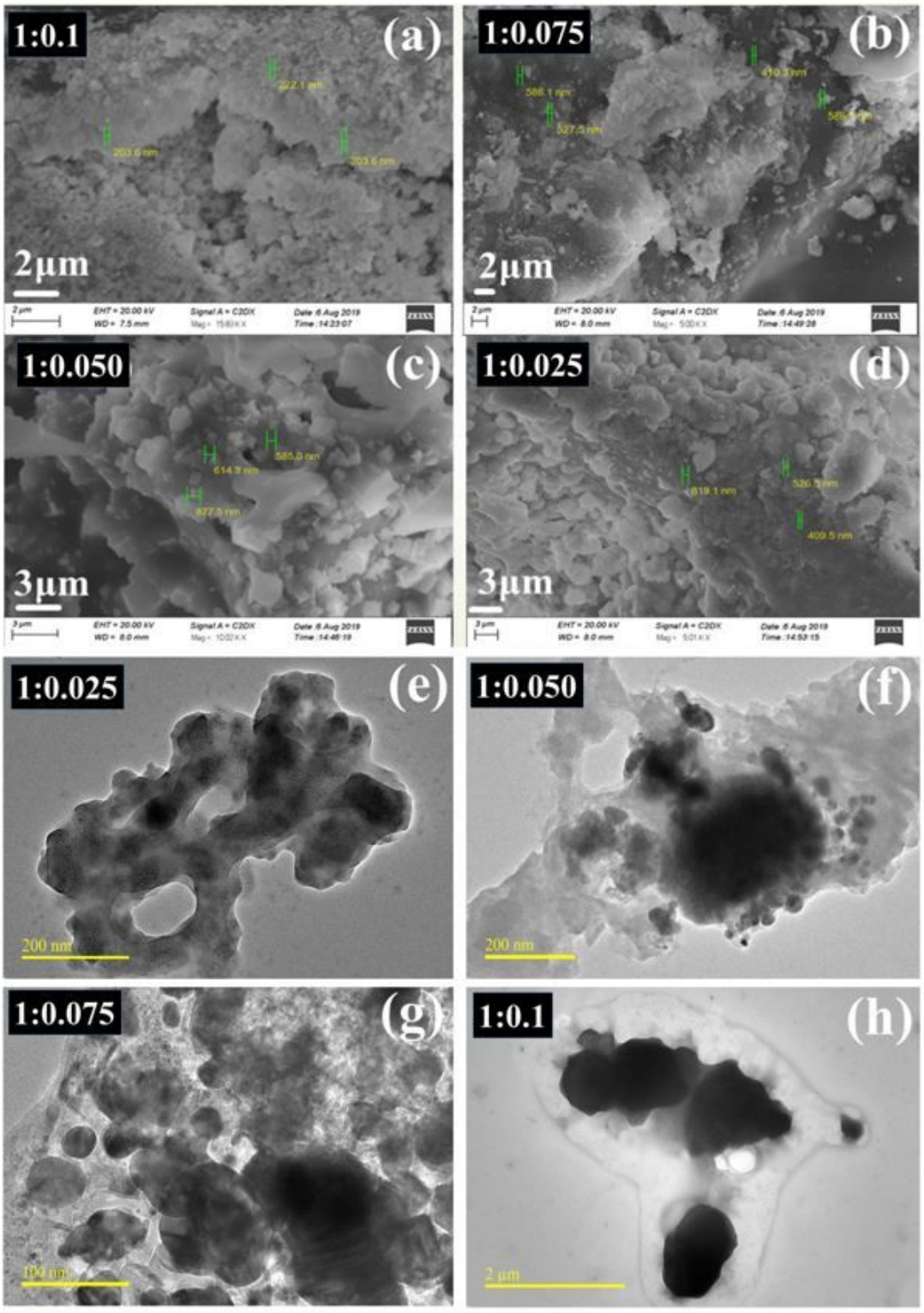

Figure 5

(a-d) SEM images obtained from prepared products (e-h) HR-TEM micrographs

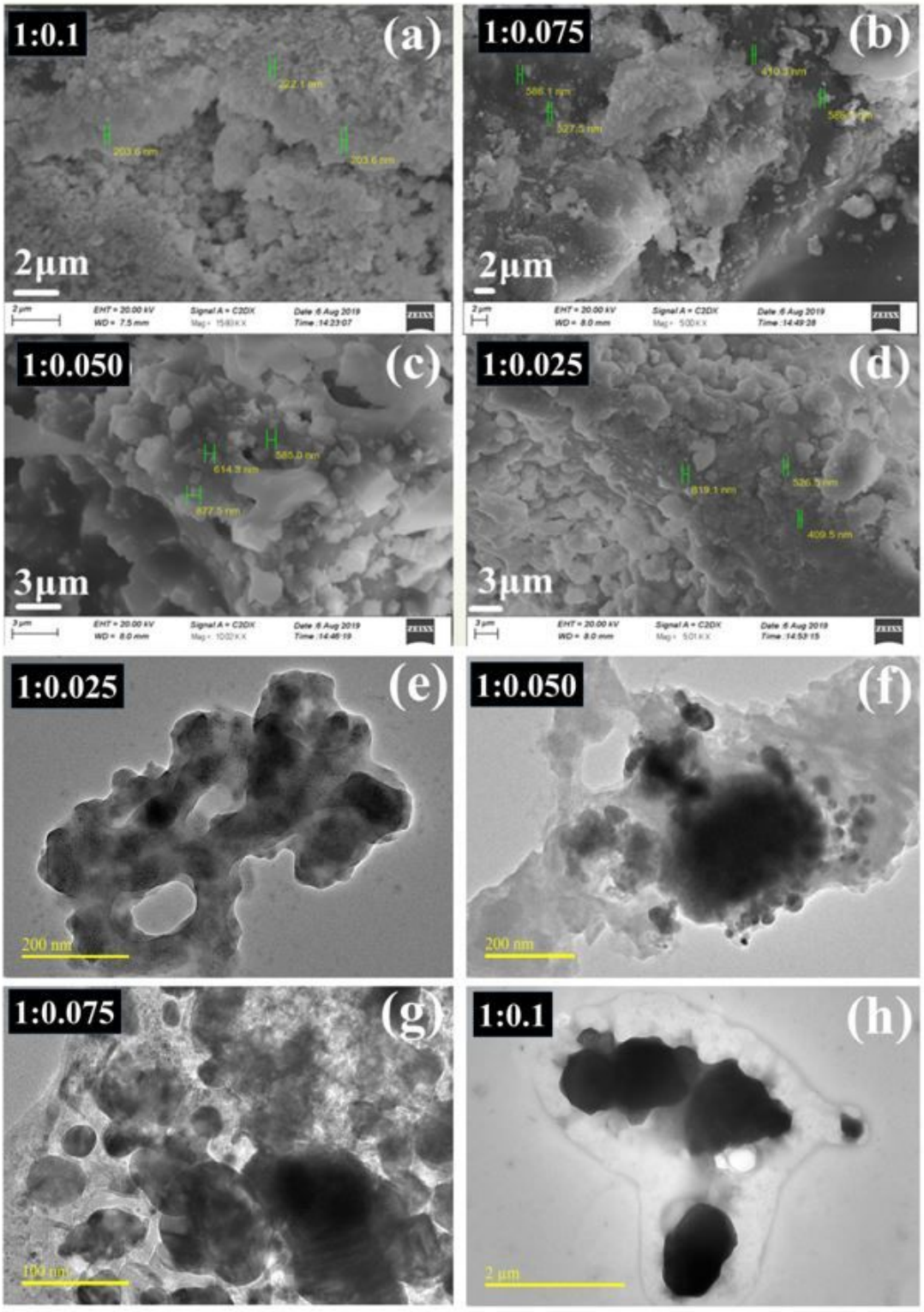

Figure 5

(a-d) SEM images obtained from prepared products (e-h) HR-TEM micrographs

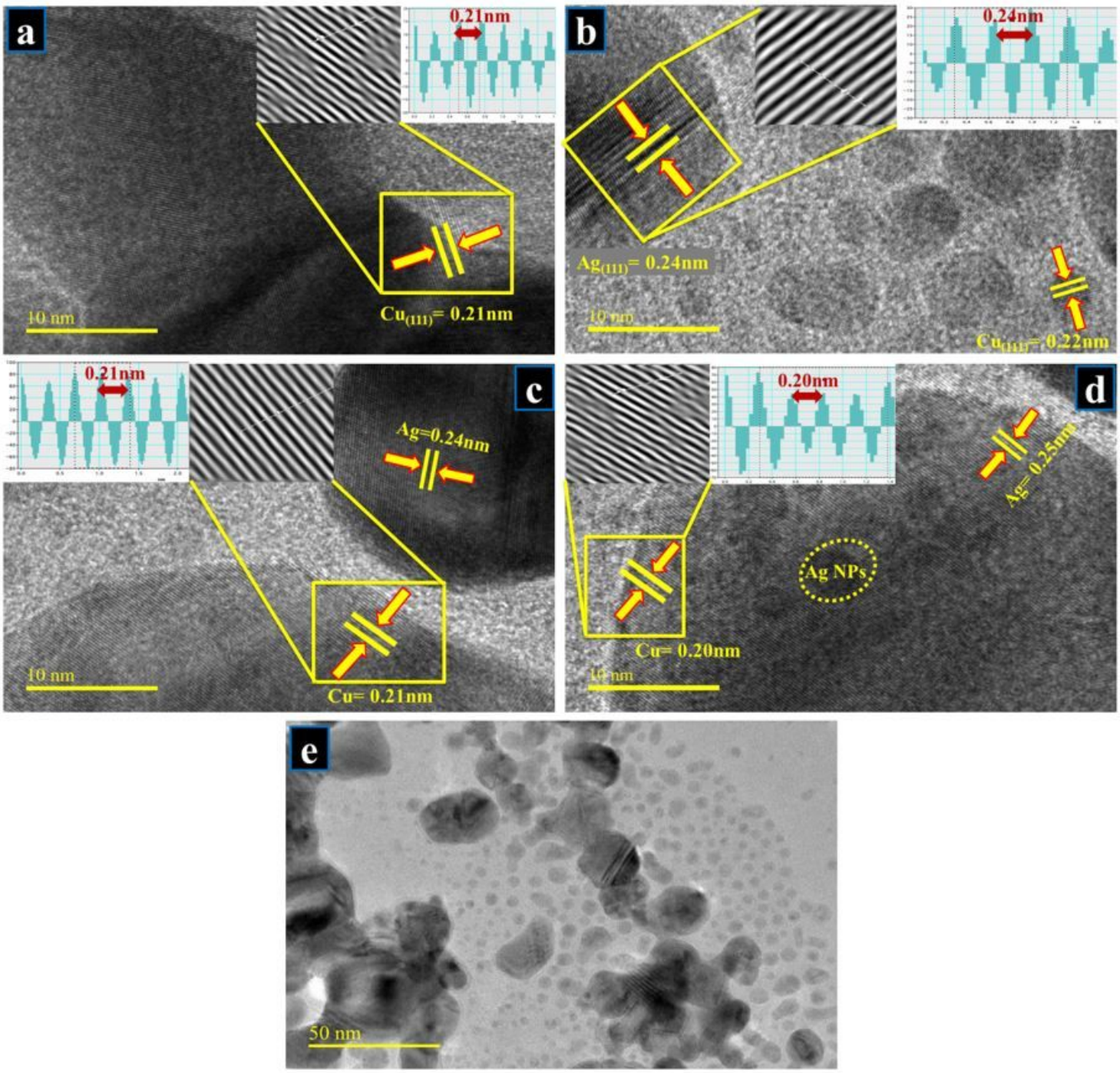

Figure 6

(a-d) HR-TEM (10 nm) images for d-spacing measurement for all prepared samples, (e) at 50 nm magnification image shows bimetallic particles.

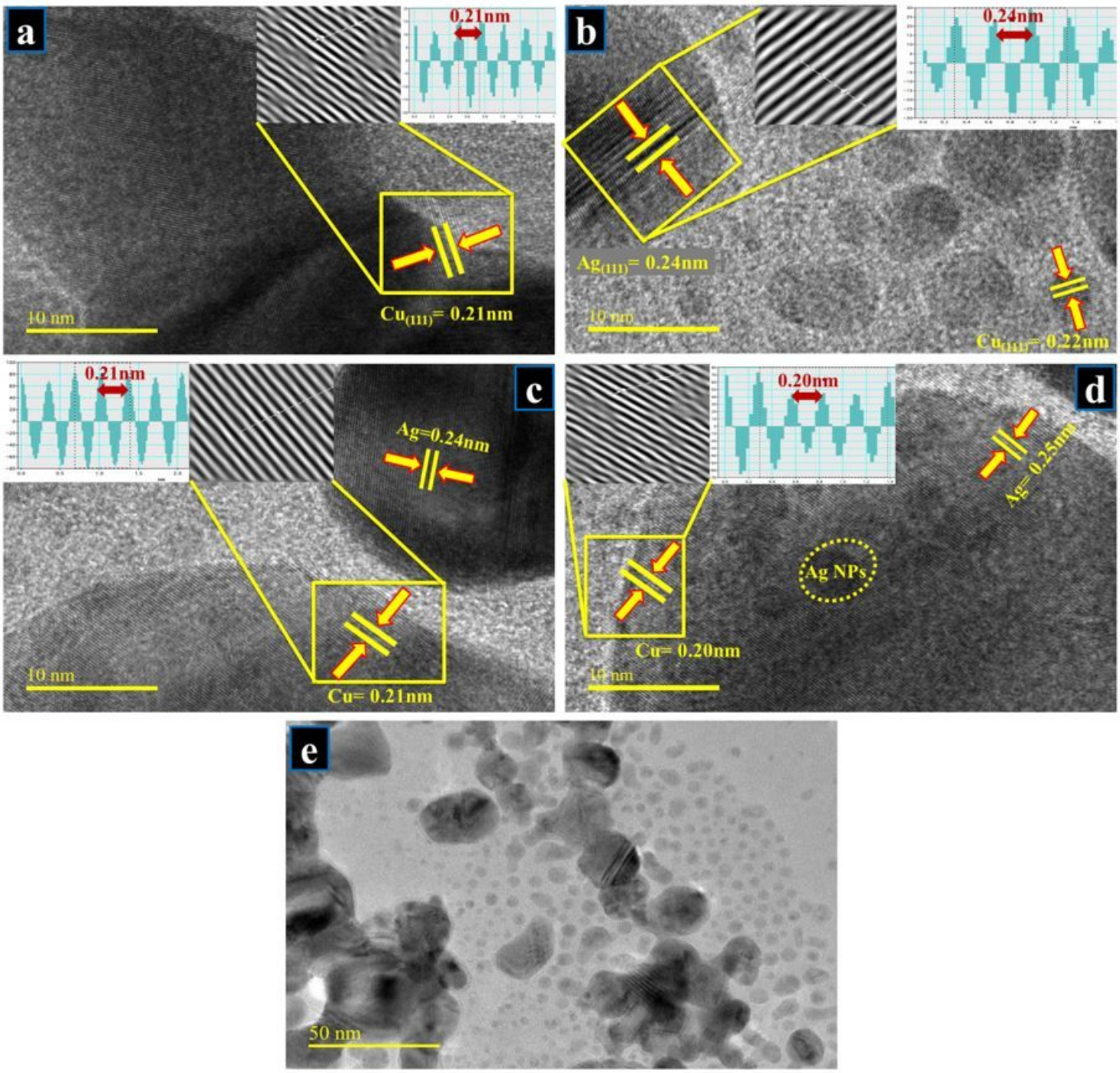

Figure 6

(a-d) HR-TEM (10 nm) images for d-spacing measurement for all prepared samples, (e) at 50 nm magnification image shows bimetallic particles.

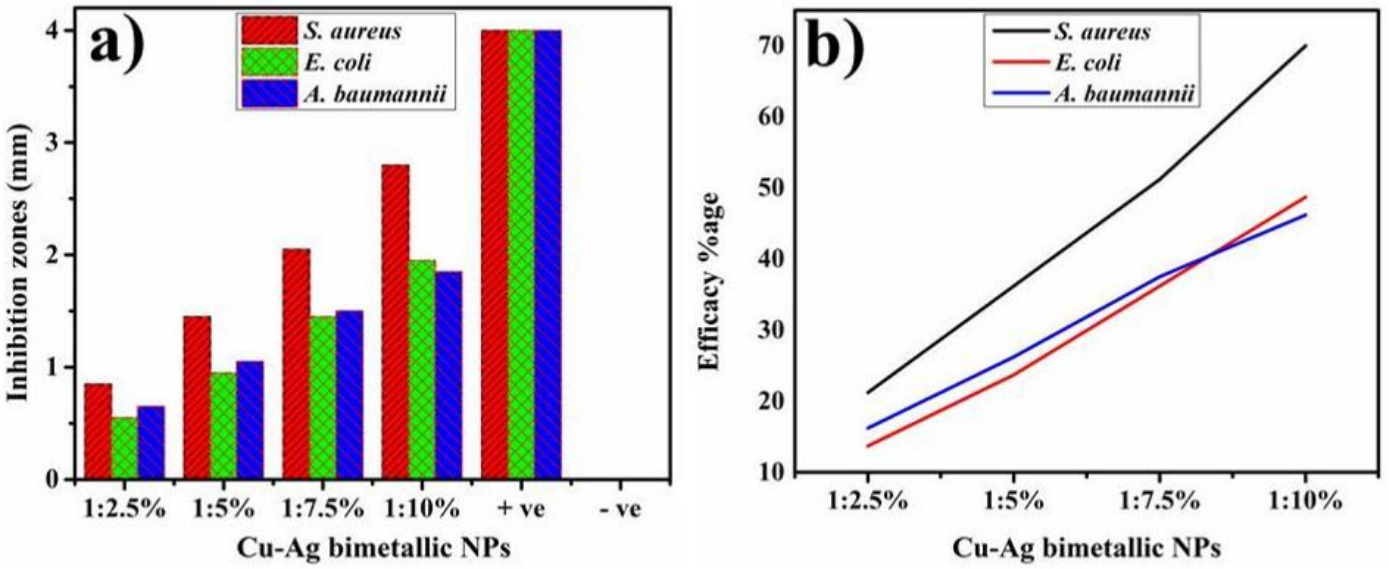

Figure 7

(a) In vitro bactericidal activity of Cu:Ag bimetallic NPs against S. aureus, E. coli and A. baumannii (b) efficacy %age, respectively

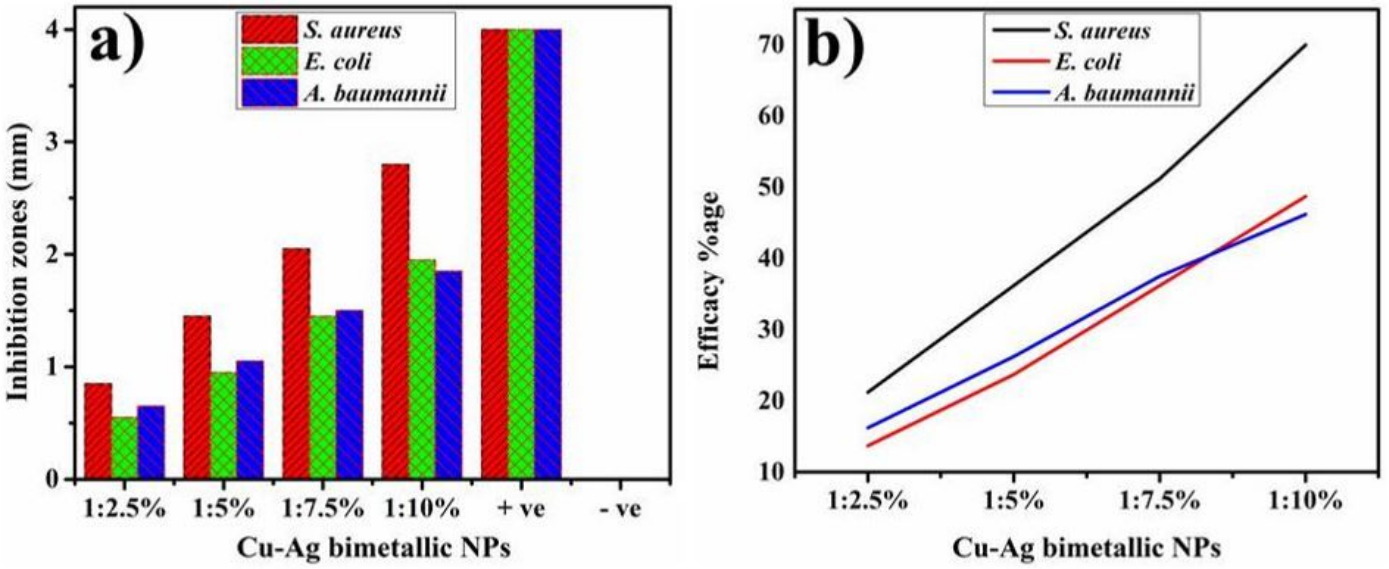

Figure 7

(a) In vitro bactericidal activity of Cu:Ag bimetallic NPs against S. aureus, E. coli and A. baumannii (b) efficacy %age, respectively

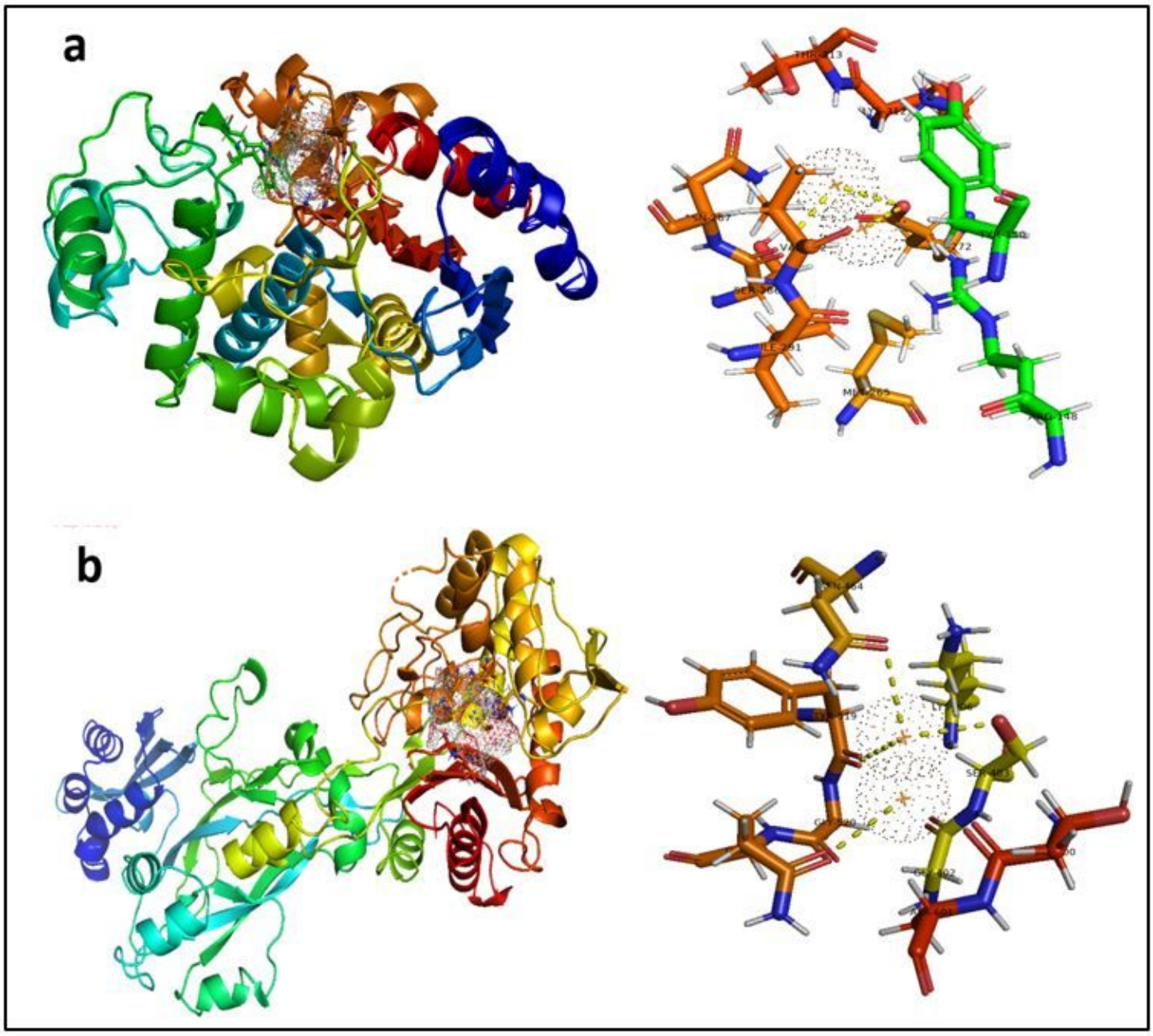

Figure 8

Binding interaction pattern of Ag-Cu Bimetallic NPs inside active pocket (a) β-lactamase from A. bauminnii, (b) β-lactamase from S. aureus

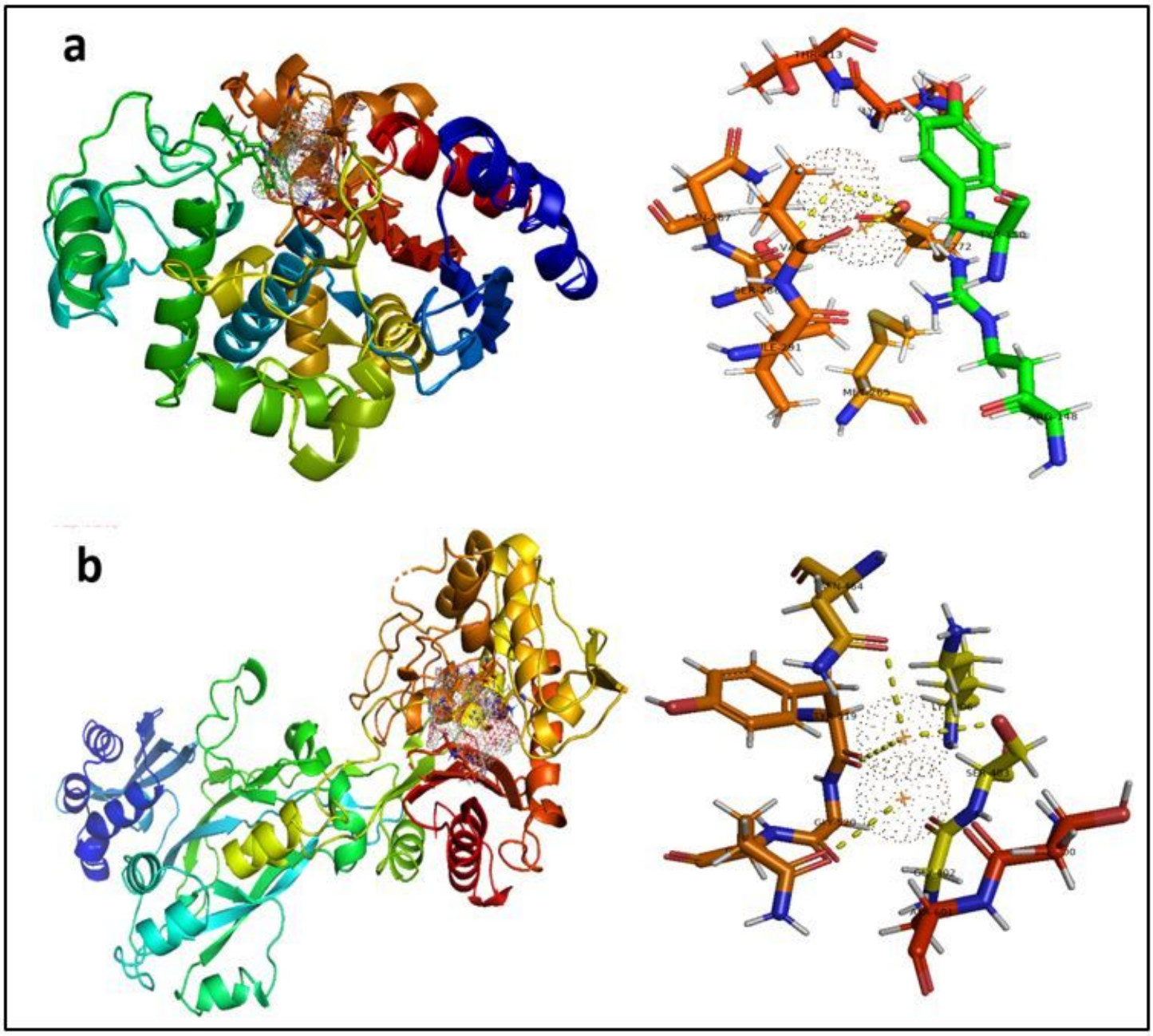

Figure 8

Binding interaction pattern of Ag-Cu Bimetallic NPs inside active pocket (a) β-lactamase from A. bauminnii, (b) β-lactamase from S. aureus

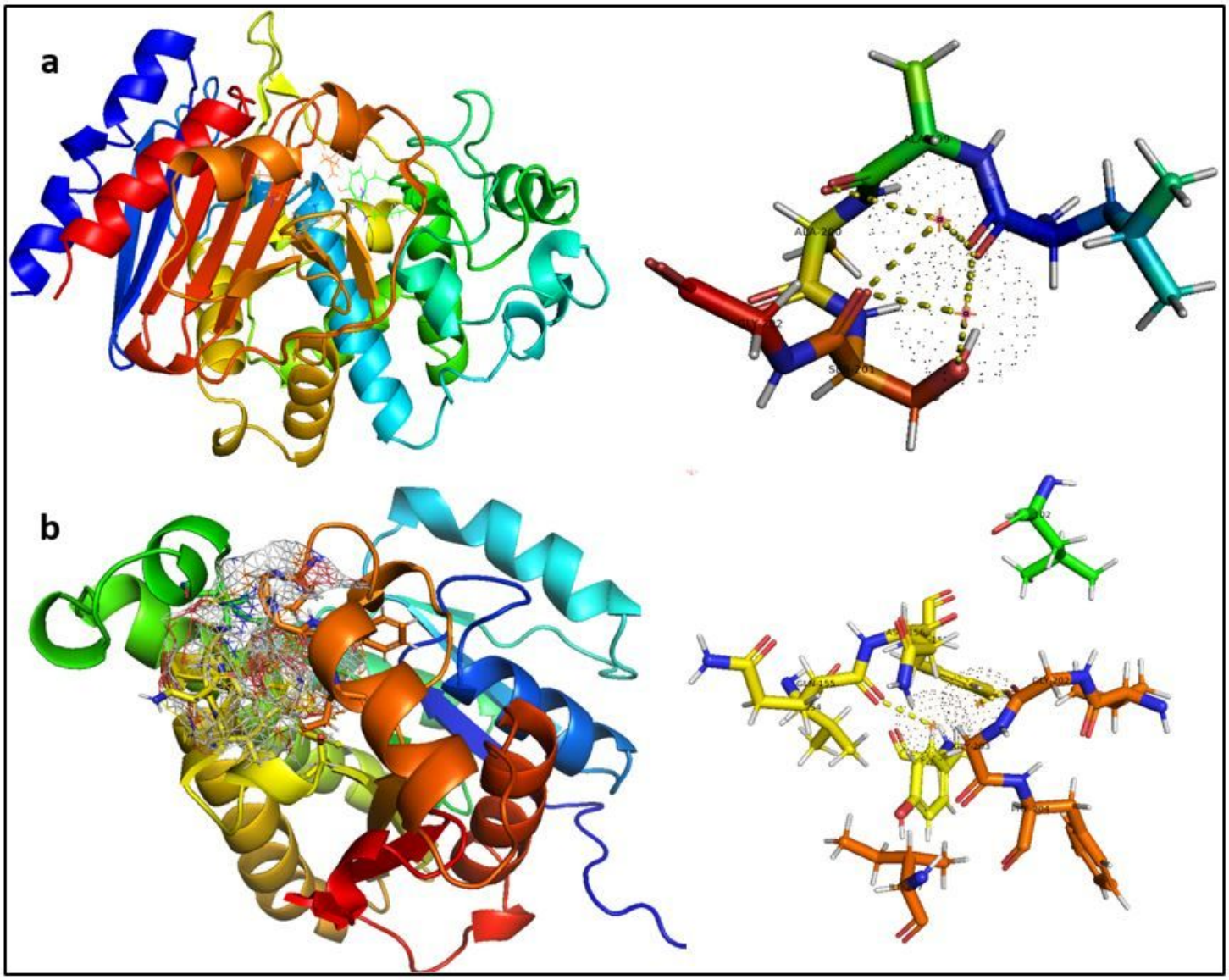

Figure 9

Binding interaction pattern of Ag-Cu Bimetallic NPs inside active pocket (a) Enoyl-[acyl-carrier-protein] reductase (FabI) from A. bauminnii, (b) Enoyl-[acyl-carrier-protein] reductase (FabI) from S. aureus

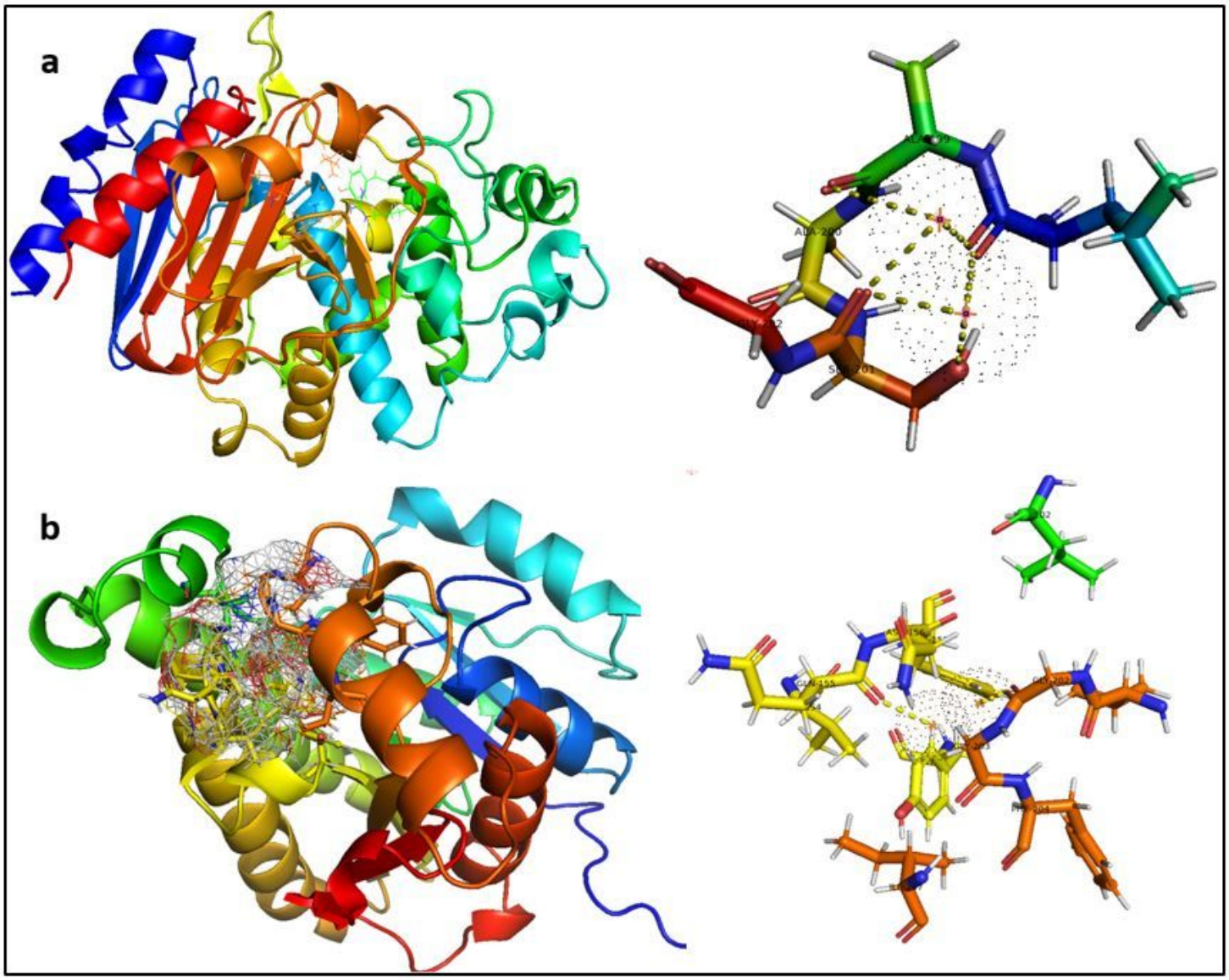

Figure 9

Binding interaction pattern of Ag-Cu Bimetallic NPs inside active pocket (a) Enoyl-[acyl-carrier-protein] reductase (FabI) from A. bauminnii, (b) Enoyl-[acyl-carrier-protein] reductase (FabI) from S. aureus

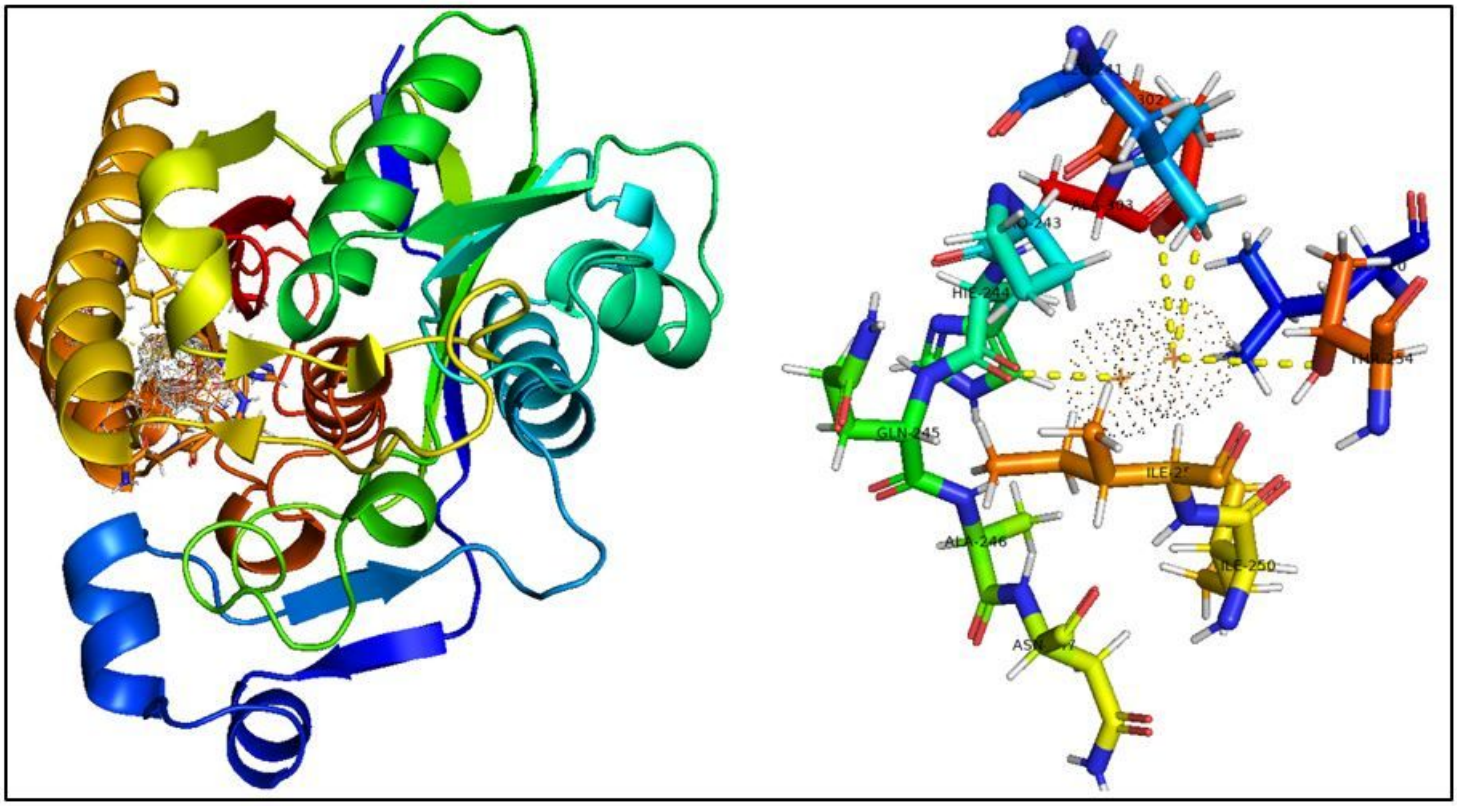

Figure 10

Binding interaction pattern of Ag-Cu Bimetallic NPs inside active pocket of FabH from E. coli

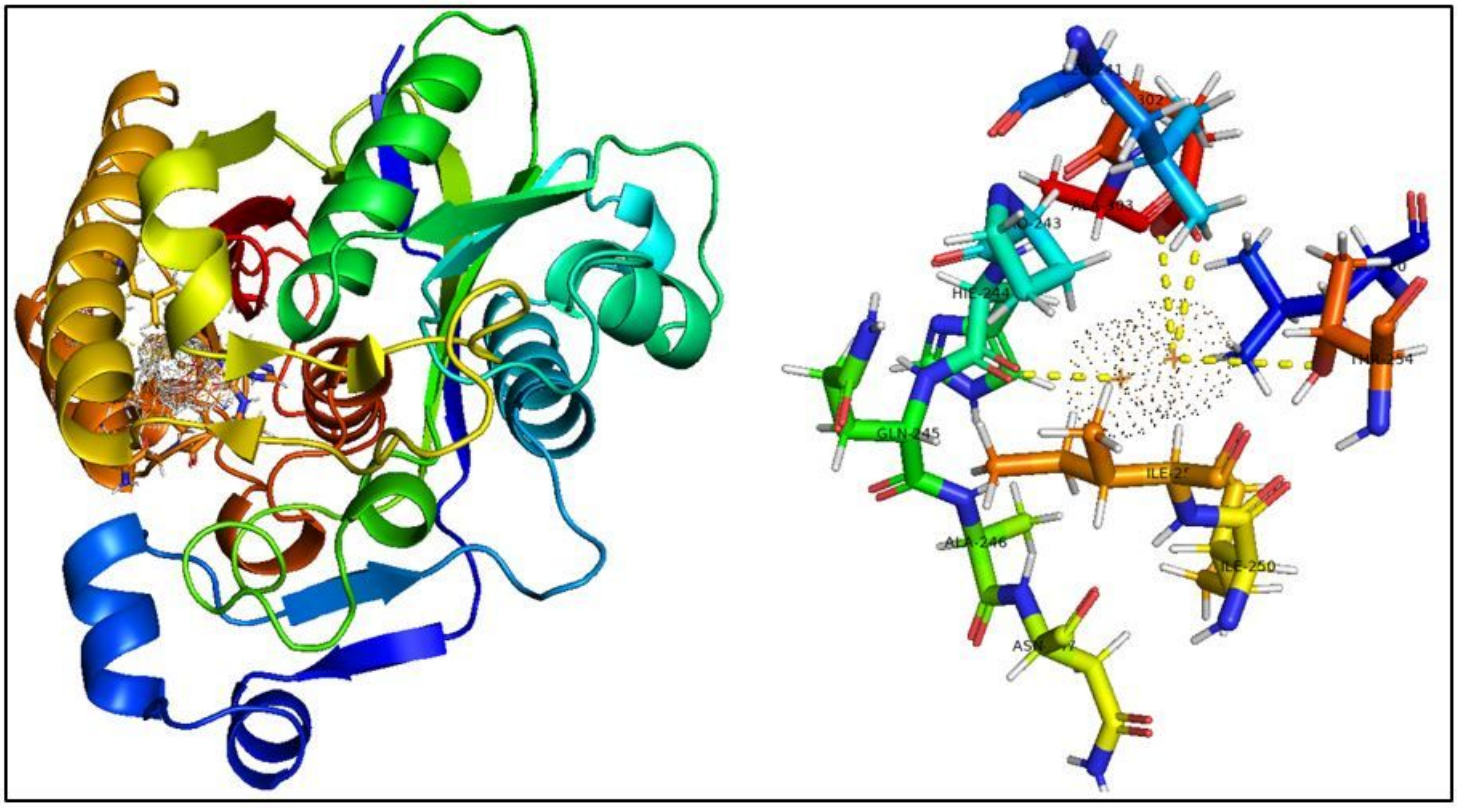

Figure 10

Binding interaction pattern of Ag-Cu Bimetallic NPs inside active pocket of FabH from E. coli